Emerging rechargeable aqueous aluminum ion battery : status, challenges, and outlooks

Yuan, Du; Zhao, Jin; Manalastas, William Jr.; Kumar, Sonal; Srinivasan, Madhavi

2020

Yuan, D., Zhao, J., Manalastas, W. J., Kumar, S. & Srinivasan, M. (2020). Emerging rechargeable aqueous aluminum ion battery : status, challenges, and outlooks. Nano Materials Science, 2(3), 248-263. https://dx.doi.org/10.1016/j.nanoms.2019.11.001

https://hdl.handle.net/10356/147558

https://doi.org/10.1016/j.nanoms.2019.11.001

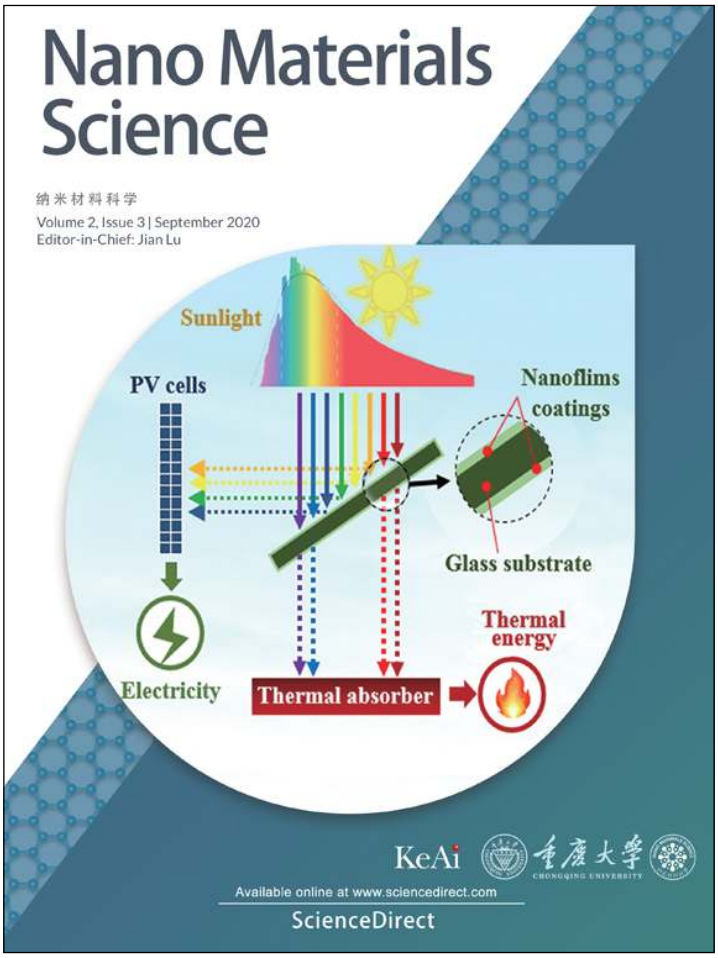

Nano Materials Science 2 (2020) 248–263

Contents lists available at ScienceDirect

Nano Materials Science

journal homepage: www.keaipublishing.com/cn/journals/nano-materials-science/

Emerging rechargeable aqueous aluminum ion battery: Status, challenges, and outlooks

Du Yuan [a,*,1], Jin Zhao [b,1], William Manalastas Jr. [b], Sonal Kumar [b], Madhavi Srinivasan [a,b,**]

[a] Energy Research Institute, Nanyang Technological University, 637553, Singapore
[b] School of Materials Science and Engineering, Nanyang Technological University, 639798, Singapore

ARTICLE INFO

Keywords:
Aluminum ion battery
Aqueous aluminum ion battery
Rechargeable
Al stripping/plating
SEI

ABSTRACT

Aluminum ion battery (AIB) technology is an exciting alternative for post-lithium energy storage. AIBs based on ionic liquids have enabled advances in both cathode material development and fundamental understanding on mechanisms. Recently, unlocking chemistry in rechargeable aqueous aluminum ion battery (AAIB) provides impressive prospects in terms of kinetics, cost, safety considerations, and ease of operation. To review the progress on AAIB, we discuss the critical issues on aluminum electrochemistry in aqueous system, cathode material design to overcome the drawbacks by multivalent aluminum ions, and challenges on electrolyte design, aluminum stripping/plating, solid-electrolyte interface (SEI) formation, and design of cathode materials. This review aims to stimulate exploration of high-performance AAIB and rationalize feasibility grounded on underlying reaction mechanisms.

1. Introduction

Continuously evolving energy demand motivates the development of lithium ion battery (LIB) and extensive application of commercial LIB products. However, limited lithium resource (0.0065 wt% of the earth's crust) urges sustainable solutions [1–3], e.g., pursuing high performance with long-term cycling stability and recycling of LIB. Also, moving towards green chemistry, alternatives to current flammable, poisonous, and volatile electrolytes for LIB are attracting great attention. Notably, aqueous LIBs have been developed, wherein water-in-salt electrolyte has achieved significant progress [4].

Responding to above calls, multivalent (MV) ion (Mg^{2+}, Ca^{2+}, Zn^{2+}, Al^{3+}) batteries are promising post-lithium candidates. MV ions are able to transfer more than one electron which leads to a high theoretical capacity and a high energy density when coupled to suitable anode. Aluminum is particularly important among MV candidates. The specific volumetric capacity of an Al anode is up to 8046 mAh cm^{-3}, close to 4 times higher compared with Li (2062 mAh cm^{-3}), with its gravimetric capacity (2980 mAh g^{-1}) comparable to that of Li metal (3860 mAh g^{-1}) [5]. Al has its high abundance, i.e., ~8 wt% of the earth crust, with low cost comparing to other candidates and low energy spent on production from minerals comparing to Li (Fig. 1) [6]. Also, the potential safety hazard is reduced for Al metal because of its better air stability compared with Li counterpart, which also benefits ease of handling in ambient environment.

Ever since aluminum primary battery were invented, utilizing Al metal anode faces the problems of hydrogen side reactions, anode corrosion, and passive oxide film formation [8]. These fatal drawbacks hinder the large-scale application of Al based battery systems. The synthesis of room temperature ionic liquids (RTILs) with wide electrochemical potential windows have enabled highly reversible Al stripping/plating, and this breakthrough has opened feasible routs to rechargeable aluminum ion battery (AIB) [2,9]. Also, nonvolatile and nonflammable ionic liquids (ILs) make so-based AIBs safe battery systems. Though with great achievement, rechargeable AIBs are impeded by fundamental scientific and technical obstructions towards high capacity and long cycling life. The principles essential for designing suitable cathodes for nonaqueous AIBs are still uncertain, especially when dealing with strong Coulombic electrostatic interaction from MV ions and solid-electrolyte interface (SEI) on Al metal. Recent success in novel electrolyte and fundamental understanding on SEI triggers the development of rechargeable aqueous aluminum ion battery (AAIB) [10,11], which

* Corresponding author.
** Corresponding author. Energy Research Institute, Nanyang Technological University, 637553, Singapore.
E-mail addresses: yuandu@ntu.edu.sg (D. Yuan), Madhavi@ntu.edu.sg (M. Srinivasan).
[1] Du Yuan and Jin Zhao contributed equally.

https://doi.org/10.1016/j.nanoms.2019.11.001
Received 20 September 2019; Accepted 6 November 2019
Available online 14 November 2019

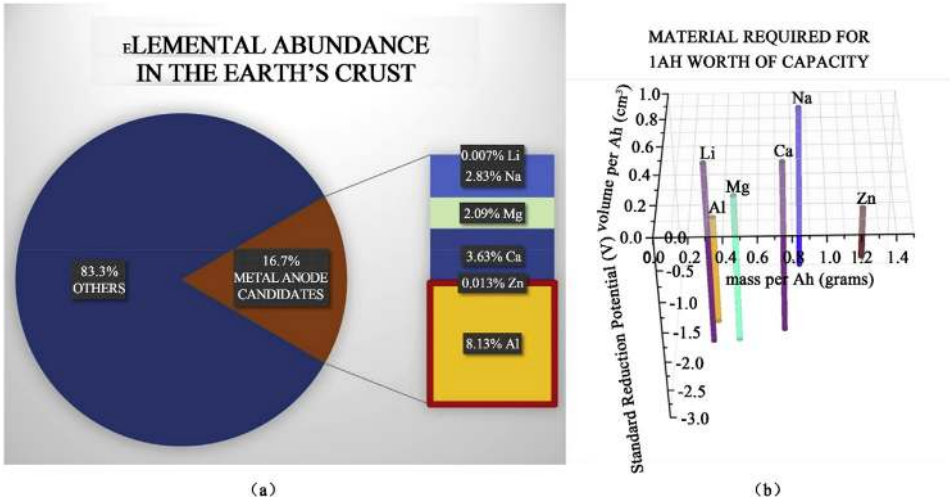

Fig. 1. Comparison on the characteristics of aluminum metal with other metals from (a) earth abundance and (b) electrochemical properties, adapted from Refs. [2,6,7].

may bring more opportunities and challenges.

Concerning rechargeable AIB, several comprehensive reviews are presented recently, which present clear picture on the development of nonaqueous rechargeable AIB [2,3,8,12–15]. In this review, we focus on the recently emerging rechargeable aqueous aluminum ion battery (AAIB). Critical issues on achieving reversible Al stripping/plating are discussed first, followed by a brief discussion on electrolyte development for Al electrochemistry. Current state-of-the-art AIB development is summarized with emphasis on cathode material design and underlying mechanisms. We then discuss the reported AAIBs on their designs and operation mechanisms. The challenges for AAIBs are further assessed in the aspects of electrolyte, Al stripping/plating, SEI, and cathode materials. Finally, we present the outlooks on pursuing reliable AAIBs with high performance.

2. Current development of aluminum ion battery (AIB)/aqueous aluminum ion battery (AAIB)

To exploit the high theoretical energy densities of AIB, utilization of metallic aluminum anode is under intensive investigation. Chemistry and electrochemistry of aluminum in aqueous system will be discussed first, followed by discussion on achieving reversible Al stripping/plating in nonaqueous system. Of note, the overall electrochemical performance of AIBs is still far from satisfactory, with reference to current LIBs. Understanding on the fundamentals drives the development of high-performance AIB, including electrochemical reaction mechanism, capacity fading mechanism of cathode, and methods to accelerate the battery kinetics. Most importantly, pioneering works on AAIBs will be discussed. Perspectives will be focused on assessment of potential cathode candidates, strategies on utilizing Al metal anode, and reaction mechanisms.

2.1. Critical issues of applying Al metal anode

Al metal anode has a highly negative standard reduction potential, i.e., −1.662V vs. SHE, compared with other metal anode candidates, which is even lower than the potential of hydrogen evolution reaction. This indicates intrinsic hydrogen evolution occurs before aluminum can be plated in the process of electrochemical reduction (Fig. 2a). Also, dilute aqueous electrolyte will decompose, where ion transport can be disrupted. Following this argument, a rechargeable AIB based on pure Al metal anode and an aqueous electrolyte (in salt-in-water regime) is unfeasible [16].

Besides the more negative reduction potential of Al^{3+}/Al than hydrogen evolution, Al metal in aqueous or protic systems exhibits fatal drawback of passivating oxide film formation as well as metal corrosion. At standard conditions, aluminum will instantaneously form a very thin (thickness ~2–10 nm), uniform, and continuous amorphous surface layer of Al_2O_3 (Fig. 2b) [20]. This oxide film is stable over a pH range of about 4.0–8.6 [21]. Although the oxide film shows advantage when using Al foil as current collector for LIB cathode with an additional contact resistance where tunneling effect facilitates the electric conduction [22,23], it provides a barrier for solvation of aluminum and transportation of aluminum ion, which poses a big challenge for using Al metal directly as anode.

Since hydroxyl ions are able to eliminate the formation of Al_2O_3 passivation layer on Al, alkaline electrolyte was applied in aluminum primary batteries where charging of Al is hindered. Utilizing Al metal in primary battery can be dated back to MnO_2|Al Leclanché battery cells [1,8]. Two types of primary cells have been constructed [13]. In the combination reaction type, e.g., Al-air (O_2) and Al–H_2O_2, aluminum takes part in cathode reaction where phase change occurs. In the hybrid reaction type, like MnO_2|Al, Al^{3+} does not participate into the cathode reaction. In alkaline system, self-discharging can not be avoided due to the spontaneous corrosion of Al. Efforts have been input to transfer primary cells away from the harsh alkaline environment. But the passivation layer forms in neutral electrolytes; hydrogen evolution is favored in acidic solutions and accelerates the self-discharging of Al metal [8].

2.2. Organic solvent

Nonaqueous electrolyte was then considered for Al metal anode, where interaction between aluminum ion and solvent species became crucial. Al^{3+} has an ionic radius of 0.0535 nm [24], and carries three positive charges. This implies that the surface charge density of Al^{3+} is more than 6 times that of Li^+ (ionic radius of 0.076 nm). Such a high surface density of aluminum ion leads to a much stronger Coulombic interaction with anions in the electrolyte. Hence, the solubility of aluminum salts in common organic solvents are significantly reduced. Consequently, ionic conductivities of the corresponding electrolytes are relatively low. In a typical ether system, strong desolvation activation energy at SEI leads to high polarization for electrodeposition [25]. When an aluminum salt with fluoric anions was used, surface of Al metal can be passivated by forming a both electronically and ionically insulating AlF_3 layer, hindering its reversible stripping/deposition [26]. Due to above points, sluggish reaction kinetics is common to AIB in nonaqueous system. In contrast, a typical working electrolyte for LIB seeks organic solvent to dissolve lithium slat properly to achieve an appreciable ionic conductivity and meanwhile coordinate cation with a relatively low

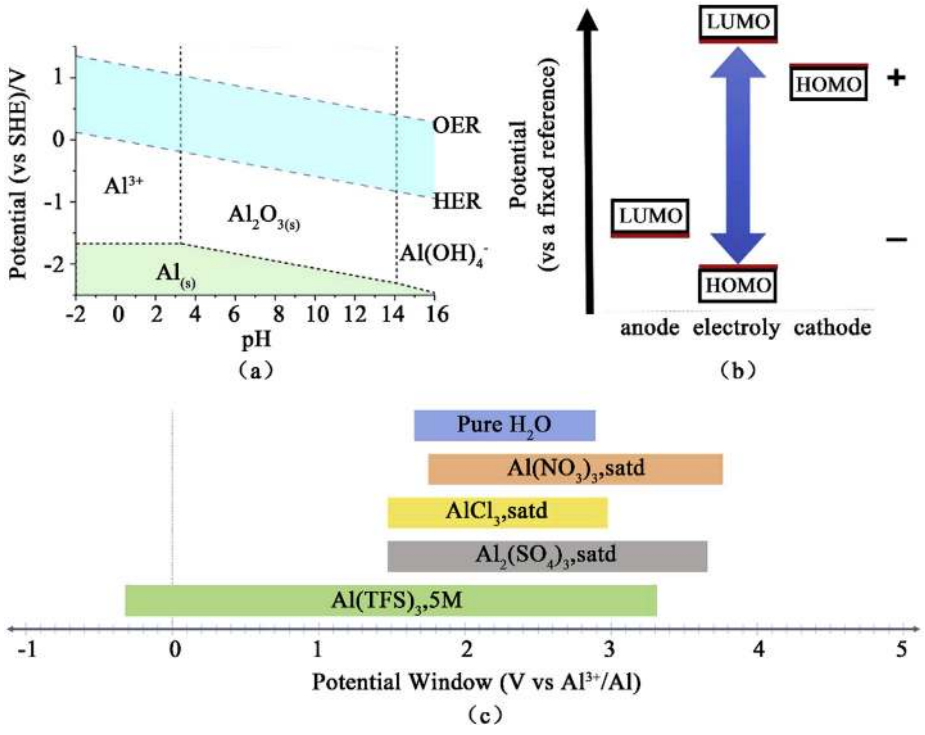

Fig. 2. (a) Pourbaix diagram of Al in 1 M aqueous aluminum salt electrolyte at 25 °C, adapted according to guideline from Refs. [17,18]. (b) Schematic diagram of electrochemical reaction potentials for an ideal battery system consisting cathode, electrolyte, and anode. (c) Summary of reported electrochemical potential windows of pure water, saturated $Al(NO_3)_3$, $AlCl_3$, and $Al_2(SO_4)_3$ [19], and $Al(OTF)_3$, 5 M [11].

desolvation activation energy allowing reversible stripping/plating [13]. It can be understood that the method for seeking a working electrolyte for LIB does not work well for AIB.

2.3. Ionic liquid

Different from solvent-solute ionization, ionic liquid (IL) adapts an molten salt synthesis approach, where conducting ions in the molten salts form via self-ionization. In early development, NaCl–$AlCl_3$ binary system and KCl–NaCl–$AlCl_3$ ternary system were applied. However, their high melting temperatures of ~180 °C are not suitable for practical applications.

The successful synthesis of room temperature ionic liquids (RTILs) facilitates reversible Al stripping/deposition, and meanwhile actuates the development of rechargeable non-aqueous AIB. At present, the RTILs predominantly used are synthesized by mixing $AlCl_3$ with imidazolium chlorides, e.g., 1-butyl-3-methylimidazolium chloride ([BMIm]Cl) and 1-ethyl-3-methylimidazolium chloride ([EMIm]Cl), at a certain ratio. Note that aluminum ions in ILs do not exist in the forms of Al^{3+} but $AlCl_4^-$ and $Al_2Cl_7^-$ [27,28]. The Al stripping/plating is based on the following equation:

$$Al + 7AlCl_4^- \leftrightarrow 4Al_2Cl_7^- + 3e^- \quad (1)$$

Hence, forming $Al_2Cl_7^-$ is critical to allow reversible Al stripping/plating, which implies a molar ratio of $AlCl_3$ to [EMIm]Cl to be more than 1. RTILs bring the advantages of their high ionic conductivities of ~10^{-3} to 10^{-2} S cm^{-1}, wide and stable electrochemical potential windows, relatively fast electrode kinetics, and enabling highly reversible stripping/plating of Al metal [2,3,8]. Fig. 3 compares the cyclic voltammetry (CV) spectra of Al stripping/plating for various electrolytes developed so far.

2.4. State-of-the-art rechargeable AIB

Based on reversible Al stripping/plating via RTILs, rechargeable AIBs based on Al metal anode were realized. Current state-of-the-art cathode materials for AIB will be discussed in this section. We extract design guidelines from the success and drawbacks of current AIBs.

2.4.1. Graphitic carbon

Graphite was firstly reported as a AIB cathode in a rechargeable graphite|$AlCl_3$/[DmPrI]Cl|Al cell by Gifford and Palmisano in 1988 [30]. However, the insufficient cycling stability and low capacity of 35–40 mAhg^{-1} hindered achieving a suitable energy density for a practical battery system, which was attributed to cathode material disintegration. The breakthrough for graphitic carbon cathode for AIB emerged in 2015 [9]. Dai and co-workers employed a 3D graphitic foam as the cathode material for AIB in acidic $AlCl_3$/[EMIm]Cl with remarkable electrochemical performance (Figs. 3c–4a). The 3D graphitic foam had covalent bonding between adjacent graphene sheets (like pyrolytic graphite), which can prevent the excessive electrode expansion causing disintegration and maintain the efficient anion intercalation. Also, the 3D structure with large pores shortened the ion diffusion length and facilitated rapid battery operation (Fig. 4b). The graphitic foam|Al cell exhibited well-defined discharge voltage plateaus ~2 V, a specific capacity of ~60 mAh g^{-1} and an impressive cycling stability of 7500 cycles with 100% capacity retention and a Coulombic efficiency (CE) of ~100% at the current density of 4 A g^{-1} (Fig. 4c), with a high rate capability, i.e. a capacity of ~60 mAh g^{-1} at the current densities from 0.1 to 5 A g^{-1}. The present cell afforded an energy density of 40 W h kg^{-1} and a high power density up to 3000 W kg^{-1}. The redox reactions during charging and discharging were proposed as below:

$$4Al_2Cl_7^- + 3e^- \leftrightarrow Al + 7AlCl_4^- \quad (2)$$

$$C_n + AlCl_4^- \leftrightarrow C_n[AlCl_4] + e^- \quad (3)$$

Where the n represents the molar ratio of carbon atoms to the intercalated anions in the graphite.

In order to match the high capacity of Al anode and thus increase the energy density of AIB, contrary approaches have been proposed to boost the capacities of graphite-/graphene-based cathodes, concerning their

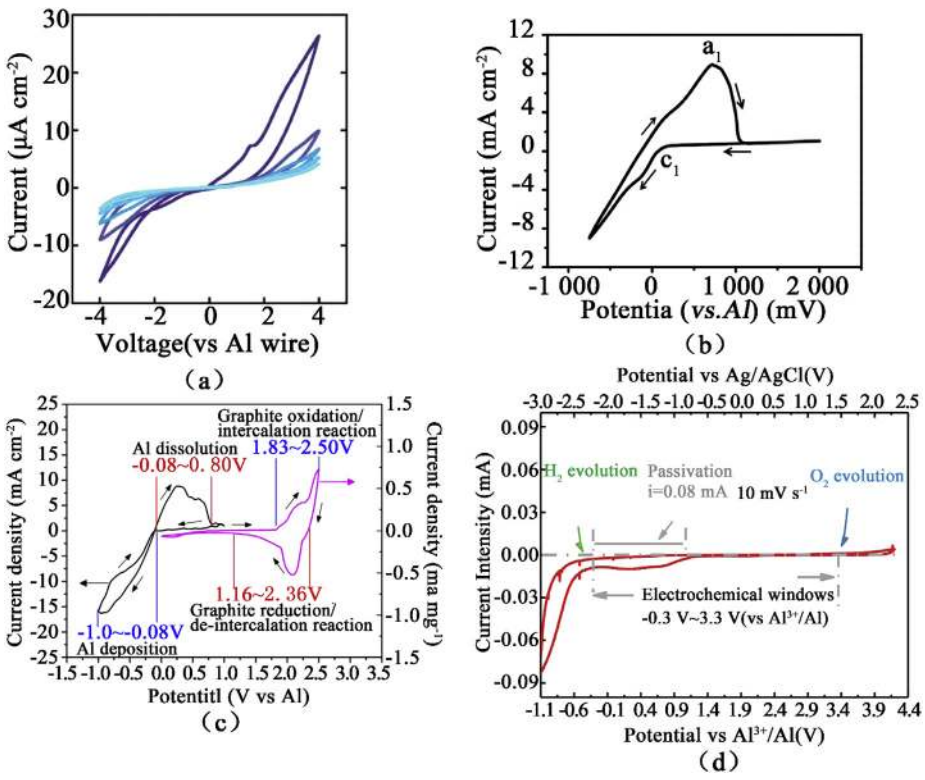

Fig. 3. The cyclic voltammograms of Al metal in (a) $Al(OTF)_3$ in diglyme, where a passivation can be seen [25]; (b) $AlCl_3$/[BMim]Cl on stainless steel with highly reversible stripping/plating [29]; (c) $AlCl_3$/[EMIm]Cl with expanded graphite [9]; and (d) 5 M $Al(OTF)_3$ [11]. (a) Reproduced with permission [25]. Copyright 2015. American Chemical Society. (b) Reproduced with permission [29]. Copyright 2018. Elsevier. (c) Reproduced with permission [9]. Copyright 2015. Springer Nature. (d) Reproduced with permission [11]. Copyright 2019. Springer Nature.

crystallinity and defects. Dai et al. developed a rechargeable AIB using free-standing SP-1 natural graphite flakes with PVDF as binder [33]. A high capacity of 110 mAh g^{-1} based on the mass of graphite was obtained at 66 mA g^{-1}. At a high rate of 660 mAg^{-1}, the capacity still maintained at 60 $mAhg^{-1}$ with a CE of ~99.5%; and at 660 mAg^{-1}, a long cycling stability over 6000 cycles was obtained without specific capacity decay with a ~99.5% CE. This study points out the necessity of high crystallinity and low defect density of graphite materials for high-performance AIB. Similarly, Gao et al. proposed a defect-free principle to design graphene cathode for AIB [31]. By annealing GO aerogel at 3000 °C, a highly crystallized defect-free few-layer graphene aerogel was obtained (Fig. 4d). The defect-free graphene aerogel delivered a high capacity of 100 mAh g^{-1} at 5 A g^{-1} with unprecedented high-rate performance (97 mAh g^{-1} at 50 A g^{-1} and 74 mAh g^{-1} at 100 A g^{-1}) and excellent cycle stability (97% capacity retention after 25 000 cycles at 5 A g^{-1}) (Fig. 4e). It reveals that the $AlCl_4^-$ anions did not intercalate into the defect sites by Raman spectra. This high temperature processing approach was also applied to prepare high-quality graphene microflower and millispheres as cathodes for high-performance AIB [34,35]. Opposite to the defect-free mechanisms, Lu et al. proposed that the nanovoids can attract and adapt more $AlCl_4^-$ ions to improve the graphene cathode capacity with experimental and theoretical evidences [35]. High quality graphene foam with nanoribbons and high porosity by Ar^+-plasma etching was formed. The obtained graphene foam afforded a high capacity of ~123 mA h g^{-1} at 5 A g^{-1} with CE higher than 98%, long cycle life of more than 10 000 cycles with no capacity decay, and high rate performance of 111 mA h g^{-1} at 8 A g^{-1}. Above opposite conclusions highlight the strong need for both fundamental experimental and theoretical studies to decouple the interfering roles of crystallinity and defects in graphite-/graphene-based cathodes.

In-depth study on intercalation unveils the importance of size and architecture on the performance of graphitic cathodes in AIB [32,36,37]. Liu et al. revealed that the behavior of chloroaluminate anion intercalation in graphitic materials (graphite and graphene) was strongly dependent on the size of graphitic material in *ab* plane and *c* direction [32]. Decreasing the vertical dimension (*c* direction) size of graphitic carbon can facilitate the kinetics of anions (de)intercalation; increasing the size of horizontal dimension (*ab* plane) can enhance the structural stability during (de)-intercalation (Fig. 4f–h). Chen et al. designed a "trihigh tricontinuous" (3H3C) graphene film cathode with features of high quality, orientation, and channeling for local structures (3H) and continuous electron-conducting matrix, ion-diffusion highway, and electroactive mass for the whole electrode (3C) [36]. This highly crystalline and porous graphene film delivered a high specific capacity of ~120 mAh g^{-1} at ultrahigh current density of 400 A g^{-1} and a ultralong cycling stability of 250 000 cycles with 91.7% capacity retention. Wu et al. prepared a monolithic 3D graphitic foam that can orient aligned graphene sheets perpendicular to the current collector substrate to facilitate ion transfer [37]. This 3D graphitic foam showed a discharge capacity of ~60 mAh g^{-1} at a high current density up to 12 A g^{-1} and a long cycling stability over 4000 cycles with CE of ~100%. This approach can avoid the extensive irreversible oxidation of graphite and prevent introducing large amounts of oxidation-induced defects into the graphene sheets.

Despite the dominant intercalation/extraction mechanism, capacitive behavior has also been reported for some carbon based cathodes, such as templated carbon, graphene aerogel, and mesoporous reduced graphene oxide [38–40]. However, the absence of discharge voltage plateaus can result in low energy densities. This should be ascribed to the high specific surface area and high content of defects as well as surface functional groups. Hence, it is essential to possess high crystallinity of carbon materials to induce intercalation reaction in AIB cathode [41–44]. Therefore, crystallinity (crystallographic dimensional specific) and defects should be well-balanced to achieve both high capacity and distinct discharge voltage plateaus. Table 1 summarizes the carbon materials based AIBs with the design of carbon materials and the respective battery performance.

2.4.2. Transition metal oxides

Though reversible intercalation of $Al_xCl_y^-$ anions in non-polar layer of graphitic carbons can deliver higher power density, the monovalent reaction inherently limits obtaining high specific capacity. To

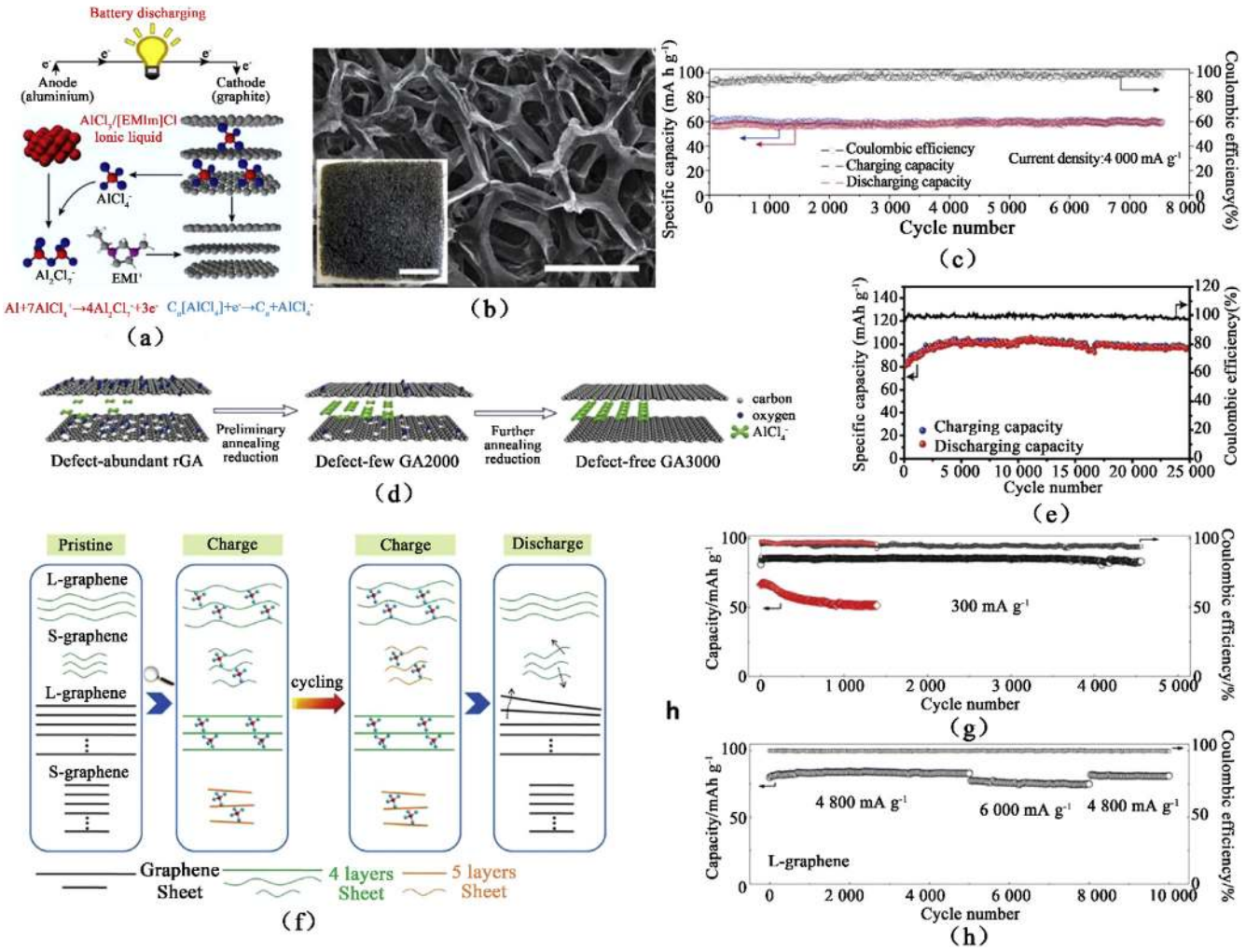

Fig. 4. (a) Schematic drawing of the graphite|$AlCl_3$/[EMIm]Cl|Al cell during discharge, where (b) Scanning electron microscopy image shows graphitic foam with an open frame structure; scale bar, 300 mm. Inset, photograph of graphitic foam; scale bar, 1 cm; with (c) Long-term stability test [9]. (d) Schematic of the defect-free design and the effect of defect content on the transportation of $AlCl^{4-}$, with (e) Galvanostatic cycling of GA-3000 (5 A g^{-1}) over 25 000 cycles [31]. (f) Schematics of aluminum ion intercalation chemistry in graphene and graphite electrodes, with (g) Cycling performances of L-graphene (black) and S-graphene (red) at a current density of 300 mA g^{-1}; and (h) Long term cycling test of an Al/L-graphene Swagelok cell at high current densities [32]. (a–c) Reproduced with permission [9]. Copyright 2015. Springer Nature. (d,e) Reproduced with permission [31]. Copyright 2017. John Wiley and Sons. (f–h) Reproduced with permission [32]. Copyright 2017. John Wiley and Sons.

accommodate the intercalation of trivalent Al^{3+} than $Al_xCl_y^-$ anions, it is essential for cathode hosts to possess moderate polarity. From this concern, transition metal oxides (transition metal = V [48–54], Ti [55–58], or Mn [10,11,59], were reported to enable accommodating intercalated Al^{3+}. The insertion of Al^{3+} in V_2O_5 was firstly investigated by Smyrl et al., in 1998 [51]. Up to 3.33 equivalents of Al^{3+} may be inserted per mole of V_2O_5 and the specific energy was estimated to be 750 W h kg^{-1} at an equilibrium potential of 1.3 V. Jayaprakash et al. reported a V_2O_5 nanowire| $AlCl_3$/[EMImCl]|Al cell delivering a discharge capacity of 305 mAh g^{-1} in the first cycle and 273 mAh g^{-1} after 20 cycles [54]. However, Reed et al. argued that the V_2O_5 nanowire was electrochemically inactive, where the measured capacity was attributed to the reaction of iron and chromium in the stainless steel current collector [60]. Later, by excluding the effects from stainless steel current collector, electrochemical activity of V_2O_5 coupled with Al has been verified [48,49,52], and V_2O_5 nanostructures have been largely explored. Wang et al. reported a binder-free cathode by directly depositing V_2O_5 on Ni foam, which delivered an initial discharge capacity of 239 mAh g^{-1}, superior to the conventional counterpart using V_2O_5 nanowires and binder [49]. The improvement was attributed to reduced electrochemical polarization. Lu et al. reported a binderless $V_2O_5{\cdot}nH_2O$ nanoflake cathode with 3D open structure, which showed good cycling stability at 100 mA g^{-1} and stable capacity of ~80 mA h g^{-1} after 100 cycles [50]. The interlayered water in V_2O_5 layers can electrostatically shield the charges of Al^{3+} for good ion mobility while the ultrathin nanoflakes make excellent contact between the electrodes and the electrolyte for short ion diffusion pathway. Besides V_2O_5, other vanadium oxides are also investigated as AIB cathode [48,53]. Channel-type B-VO_2 was evaluated to deliver a discharge capacity of 116 mAh g^{-1} after 100 cycles at 50 mA g^{-1} [53]. Li_3VO_4@C microsphere was designed where the empty sites in the hollow lantern-like 3D Li_3VO_4 structure can accommodate ions inserting reversibly while the carbon layer can increase the electrode conductivity and restrain the volume expansion [48]. Li_3VO_4@C exhibited an initial discharge capacity of 137 mAh g^{-1} and remained at 48 mAh g^{-1} after 100 cycles with almost 100% CE at 20 mA g^{-1}.

Metal oxides such as CuO, MoO_2 and molybdenum–vanadium oxide were also investigated for AIB [61–63]. Table 2 provides a short summary on representative metal oxides for cathodes in AIB. On the other hand, charge storage of Al^{3+} in TiO_2 has been intensively studied in aqueous electrolyte. Also, investigation on MnO_2 for aqueous system has been conducted recently. Detailed discussion on the underlying

Table 1
Electrochemical performance of carbon materials for AIB cathodes.

Cathode	Anode	Electrolyte	Discharge voltage	Capacity /Current	Rate/Current	Retention (% at cycles)	Ref.
Zeolite-templated carbon	Al	$AlCl_3$/[EMIm]Cl	average 1.05 V	382 mAh g^{-1} /0.05 A g^{-1}	186 mAh g^{-1} /1 A g^{-1}	86% at 1000	[38]
Kish Graphite Flakes	Al	$AlCl_3$/[EMIm]Cl	average 1.79 V	142 mAh g^{-1} /0.05 A g^{-1}	124 mAh g^{-1} /10 A g^{-1}	~100% at 200	[45]
Graphene film	Al	$AlCl_3$/[EMIm]Cl	–	240 mAh g^{-1} /1 A g^{-1}	90 mAh g^{-1} /10 A g^{-1}	~100% at 5000	[39]
Mesoporous rGO	Al	$AlCl_3$/[EMIm]Cl	–	120 mAh g^{-1} /0.2 A g^{-1}	20 mAh g^{-1} /20 A g^{-1}	~85% at 100	[40]
Carbon paper	Al	$AlCl_3$/[EMIm]Cl	~1.8 V	85 mAh g^{-1} /0.05 A g^{-1}	63 mAh g^{-1} /0.15 A g^{-1}	–	[46]
Graphene microflower	Al	$AlCl_3$/[EMIm]Cl	average ~ 1.85 V	~92 mAh g^{-1} /0.1 A g^{-1}	100 mAh g^{-1} /20 A g^{-1}	~100% at 5000	[47]
Defect-free graphene	Al	$AlCl_3$/[EMIm]Cl	average ~ 1.94 V	100 mAh g^{-1} /5 A g^{-1}	74 mAh g^{-1} /100 A g^{-1}	97% at 25000	[31]
Large-sized few-layer graphene	Al	$AlCl_3$/[PMIm]Cl	–	90 mAh g^{-1} /0.3 A g^{-1}	90 mAh g^{-1} /4.8 A g^{-1}	100% at 10000	[32]
Graphene nanoribbons on highly porous 3D graphene	Al	$AlCl_3$/[EMIm]Cl	~2 V	148 mAh g^{-1} /2 A g^{-1}	111 mAh g^{-1} /8 A g^{-1}	98% at 10000	[35]
3D graphitic foams	Al	$AlCl_3$/[EMIm]Cl	~1.8 V	60 mAh g^{-1} /2 A g^{-1}	60 mAh g^{-1} /12 A g^{-1}	100% at 4000	[37]
Graphene film	Al	$AlCl_3$/[EMIm]Cl	2.3 to 2.0 V and 2.0 to 1.5 V	120 mAh g^{-1} /6 A g^{-1}	120 mAh g^{-1} /400 A g^{-1}	91.7% at 250000	[36]
Carbon nanoscrolls	Al	$AlCl_3$/[EMIm]Cl	–	104 mAh g^{-1} /1 A g^{-1}	101 mAh g^{-1} /10 A g^{-1}	100% at 55000	[42]
3D graphitic-foam	Al	$AlCl_3$/[EMIm]Cl	2 V	~70 mAh g^{-1} /1 A g^{-1}	~60 mAh g^{-1} /6 A g^{-1}	100% at 7500	[9]
Natural graphite	Al	$AlCl_3$/[EMIm]Cl	2.25–2.0 V and 1.9–1.5 V	110 mAh g^{-1} /0.066 A g^{-1}	~60 mAh g^{-1} /0.66 A g^{-1}	100% at 6000	[33]
Carbon nanofibers	Al	$AlCl_3$/[EMIm]Cl	–	126 mAh g^{-1} /1 A g^{-1}	95 mAh g^{-1} /50 A g^{-1}	100% at 20000	[43]

Table 2
Electrochemical performance of representative metal oxides for AIB cathodes.

Cathode	Anode	Electroyte	Discharge voltage	Capacity /Current	Rate/ Current	Retention (% at cycles)	Ref.
Li_3VO_4@C	Al	$AlCl_3$/[EMIm]Cl	~0.5 V	137 mAh g^{-1} /0.02 A g^{-1}	–	~35% at 100	[48]
VO_2	Al	$AlCl_3$/[BMIm]Cl	~0.5 V	116 mAh g^{-1} /0.05 A g^{-1}	70 mAh g^{-1} /0.2 A g^{-1}	~70% at 100	[53]
V_2O_5/C	Al	Mixture of $AlCl_3$, dipropylsulfone and toluene	~1 V	200 mAh g^{-1} /0.01 A g^{-1}	50 mAh g^{-1} /0.04 A g^{-1}	~66% at 15	[64]
V_2O_5 nanowires	Al	$AlCl_3$/[BMIm]Cl	~0.5 V	–	–	~50% at 10	[52]
V_2O_5 nanowires	Al	$AlCl_3$/[EMIm]Cl	~0.55 V	305 mAh g^{-1} /-	–	~78% at 20	[54]
V_2O_5	Al	$AlCl_3$/[BMIm]Cl	~0.6 V	239 mAh g^{-1} /-	–	–	[49]
Porous CuO microsphere	Al	$AlCl_3$/[EMIm]Cl	~0.6 V	250 mAh g^{-1} /0.05 A g^{-1}	235 mAh g^{-1} /0.2 A g^{-1}	~45% at 100	[61]
MoO_2	Al	$AlCl_3$/[EMIm]Cl	~1.95 V	90 mAh g^{-1} /0.1 A g^{-1}	–	~28% at 100	[62]
open framework $Mo_{2.5+y}VO_{9+z}$	Al	$AlCl_3$/[BMIm]Cl	~0.75 V	340 mAh g^{-1} /0.002 A g^{-1}	150 mAh g^{-1} /0.02 A g^{-1}	–	[63]

electrochemical reaction mechanism for the above systems will be elaborated in Section 2.(v).

2.4.3. Metal sulfides

Metal sulfides are expected to outperform oxides in MV cation insertion because of ameliorated electrostatic interactions with guest ions, weaker Al–S bonds compared with ultrastable Al–O, and increased conductivities. Generally, the aluminum storage mechanism in metal sulfides can be divided in to insertion and conversion reaction mechanisms [3]. In 1980, a FeS_2|Al rechargeable AIB was proposed without establishing a detailed reaction mechanism [65]. Later in 2016, Mori et al. re-investigated FeS_2 and proposed the discharge reaction mechanism as [66]:

$$FeS_2 + 2/3Al^{3+} + 2e^- \rightarrow FeS + 1/3Al_2S_3 \quad (4)$$

By novel composite cathode design, a Ni_3S_2/graphene|$AlCl_3$/[EMIm]Cl|Al cell was reported [67]. It was found the dissociation process of $Al_2Cl_7^-$ during charge process, where the active material transformed from monocrystal to polycrystal. An initial discharge specific capacity of 350 mAh g^{-1} at a current density of 100 mA g^{-1} was achieved, and the discharge capacity remained over 60 mAh g^{-1} with CE of 99% after 100 cycles. Later, a 3D CuS@C was reported for AIB, with the following discharge/charge mechanism [68]:

In the discharge process:

Cathode: $6CuS + 2Al^{3+} + 6e^- \rightarrow 3Cu_2S + Al_2S_3$ (5)

Anode: $Al + 7AlCl_4^- - 3e^- \rightarrow 4Al_2Cl_7^-$ (6)

In the charge process:

Cathode: $3Cu_2S + Al_2S_3 - 6e^- \rightarrow 6CuS + 2Al^{3+}$ (7)

Anode: $4Al_2Cl_7^- + 3e^- \rightarrow Al + 7AlCl_4^-$ (8)

The battery showed a high average voltage of ~1.0 V and delivered a capacity of ~90 mAh g^{-1} with nearly 100% CE after 100 cycles at 20 mA g^{-1}. Intercalation reaction for Al^{3+} storage in $aMo_6S_8|AlCl_3$/[BMIm]Cl|Al cell was also reported, with the Al intercalation capacity of 167 mAh g^{-1} (equivalent to a formula of $Al_{1.73}Mo_6S_8$) at 2.4 mA g^{-1} [69]. SnS_2 and SnS were also investigated as intercalation type cathodes for AIBs [70,71]. A self-supported SnS porous film was fabricated as flexible cathode, where the porous structure was designed to minimize the volume expansion during charge/discharge [70]. This porous SnS cathode delivered a high reversible specific capacity of 406 mAh g^{-1} at 20 mA g^{-1} and a long cycling stability of 1000 cycles with a capacity decay rate of 0.03% per cycle at 100 mA g^{-1}. A summary of the representative metal sulfides as AIB cathodes is presented in Table 3.

Due to the high energy density (1340 Whkg^{-1}) and low cost, the Al|S system is also proposed as a very promising battery system for electric vehicles and grid energy storage. Current efforts shed light on the electrochemical reaction of sulfur in a trivalent cation environment and facilitate the progress on the way to realize rechargeable Al|S batteries [75–79].

2.4.4. Metal selenides

Selenium is introduced into the family of rechargeable batteries because of its comparable chemical properties to sulfur. Se has similar electrochemical properties to S, but a lower ionization potential (9.7 eV vs 10.4 eV) which facilitates its easier electrochemical oxidation [80]. Besides, its high electronic conductivity enables a reduced overpotential and its high volumetric capacity of 3247 mAh cm^{-3} favors fabricating Se based batteries in limited spaces. Huang et al. reported the very first Se|Al battery in a composite of Se nanowires and mesoporous carbon (CMK-3)|$AlCl_3$/[EMIm]Cl|Al cell [81]. A unique mechanism was proposed where CMK-3 nanorods played a dual role, i.e., acted as a reservoir to capture Se_2Cl_2 generated by Se reacting with $AlCl_4^{-1}$ and helped to confine Se_2Cl_2 in its pores to avoid dissolution of Se_2Cl_2 into the electrolyte and facilitates subsequent charge/discharge. The following overall reaction was proposed.

$2Se + 4AlCl_4^- \leftrightarrow Se_2Cl_2 + 2Al_2Cl_7^-$ (9)

Further, electrochemistry of the Se|Al system was studied based on two-electron transfer (Se^0 to Se^{2-}) with the following proposed reactions [82]:

Discharge process:

Cathode: $3Se + 8Al_2Cl_6Br^- + 6e^- \rightarrow Al_2Se_3 + 8AlCl_3Br^- + 6AlCl_4^-$ (10)

Anode: $2Al + 8AlCl_3Br - + AlCl_4^- - 6e - \rightarrow 8Al_2Cl_6Br -$ (11)

Charge process:

Cathode: $Al_2Se_3 + 8AlCl_3Br - + AlCl_4^- - 6e - \rightarrow 3Se + 8Al_2Cl_6Br -$ (12)

Anode: $8Al_2Cl_6Br^- + 6e^- \rightarrow 2Al + 8AlCl_3Br^- + 6AlCl_4^-$ (13)

Overall: $2Al + 3Se \rightleftharpoons Al_2Se_3$ (14)

It shows that the complex $Al_2Cl_6Br^-$ dissociated into $AlCl_3$ and $AlCl_3Br^-$ intermediates which further generated the Al^{3+} ions that react with Se to form Al_2Se_3. First-principle calculations indicate lower overall activation energy needed for above reactions as compared to energy needed for dissociation of $Al_2Cl_7^-$, which effectively enables efficient and fast reactions between Al and Se.

Al^{3+} intercalation/extraction has also been studied in metal selenide based AIBs. One-dimensional $Cu_{2-x}Se$ nanorods were developed with non-stoichiometry, large cell volume, and ultrahigh electronic conductivity, which delivered an initial capacity of 241 mAh g^{-1} that maintained at 100 mAh g^{-1} after 100th cycle [83]. Nanoporous carbon-encapsulated CoSe derived from metal-organic frameworks derived showed high capacity of 427 mAh g^{-1} at 1 A g^{-1} and 254.8 mAh g^{-1} at 5 A g^{-1} [84]. The superior performance at high rate was attributed to the large lattice spacing of CoSe nanoparticles allowing for easy Al^{3+} insertion, shorter diffusion distance allowing for better kinetics, and 3D interlinked open structure allowing for better electrolyte infiltration and structural integrity. It further reveals that incorporation of aluminum ion in $CoSe_2$ caused partial substitution of Co^{2+} by Al^{3+}, leading to the formation of $Al_mCo_nSe_2$ along with elemental Co. In parallel, dissolution of active cobalt species and pulverization of $CoSe_2$ were identified to be the main reasons for capacity fading. To tackle dissolution, a conductive wrapping layer of reduced graphene oxide was used which imparted various functionalities including protection of $CoSe_2$/carbon nanodice composites from cobalt dissolution and $CoSe_2$ pulverization along with enhanced conductivity, where long cycling stability of over 500 cycles was achieved with a capacity of 143 mAh g^{-1} at 1 A g^{-1} [85]. Similar to CoSe, α-MnSe microspheres were also studied for Al

Table 3
Electrochemical performance of representative metal sulfides for AIB cathodes.

Cathode	Anode	Electroyte	Discharge voltage	Capacity /Current	Rate/Current	Retention (% at cycles)	Ref.
TiS_2	Al	$AlCl_3$/[BMIm]Cl	–	~50 mAh g^{-1} /0.005 A g^{-1}	–	~72% at 50	[72]
$Cu_{0.31}Ti_2S_4$	Al	$AlCl_3$/[BMIm]Cl	–	~95 mAh g^{-1} /0.005 A g^{-1}	–	~16% at 50	[72]
Hexagonal NiS nanobelts	Al	$AlCl_3$/[EMIm]Cl	~0.9 V	~105 mAh g^{-1} /0.02 A g^{-1}	83.6 mAh g^{-1} /0.3 A g^{-1}	~100% at 100	[73]
VS_4/rGO	Al	$AlCl_3$/[EMIm]Cl	–	~407 mAh g^{-1} /0.1 A g^{-1}	~203 mAh g^{-1} /0.3 A g^{-1}	~20% at 100	[74]
Mo_6S_8	Al	$AlCl_3$/[BMIm]Cl		~80 mAh g^{-1} /0.006 A g^{-1}	~25 mAh g^{-1} /0.12 A g^{-1}	~47% at 50	[69]
SnS_2/rGO	Al	$AlCl_3$/[EMIm]Cl	~0.68 V	392 mAh g^{-1} /0.1 A g^{-1}	112 mAh g^{-1} /1 A g^{-1}	~25% at 100	[71]
SnS porous film	Al	$AlCl_3$/[EMIm]Cl	~1.1 V	406 mAh g^{-1} /0.02 A g^{-1}	160.5 mAh g^{-1} /0.5 A g^{-1}	~91% at 100	[70]
CuS@C microsphere	Al	$AlCl_3$/[EMIm]Cl	~1 V	90 mAh g^{-1} /0.02 A g^{-1}	~161 mAh g^{-1} /0.1 A g^{-1}	~32% at 100	[68]
Ni_3S_2@ Graphene	Al	$AlCl_3$/[EMIm]Cl	~1 V	350 mAh g^{-1} /0.1 A g^{-1}	235 mAh g^{-1} /0.2 A g^{-1}	~17% at 100	[67]

intercalation/extraction, which showed a capacity of 408 mAh g^{-1} at 0.2 A g^{-1}, with its porous nanostructure overcoming large volume expansion and poor diffusion kinetics [86].

2.4.5. Other candidates

Besides carbon materials, metal oxides, and metal sulfides, other types of cathodes materials for AIBs are also being investigated. Due to their open structure, Prussian blue analogs (PBAs) (e.g., copper hexacyanoferrate) are promising for aluminum ion insertion/extraction [87,88]. Phosphates with tunneling channels and much larger d-spacing than the radius of Al^{3+} could be promising cathode candidate. Porous $Co_3(PO_4)_2$@C composites derived from ZIF-67 was reported in a $Co_3(PO_4)_2$@C|$AlCl_3$/[EMIm]Cl|Al cell [89]. Al^{3+} could efficiently intercalate and be extracted in the lattice of $Co_3(PO_4)_2$ tunnel structure with reversible formation of $Al_mCo_n(PO_4)_2$. The porous $Co_3(PO_4)_2$@C exhibited excellent electrochemical kinetics and ultrahigh cycling stability with superior capacity of 151 mA h g^{-1} at the current density of 2 A g^{-1} after 500 cycles and a capacity decay of only 0.02% per cycle as well as high specific capacity of 111 mA h g^{-1} at 6 A g^{-1}. Moreover, the storage capabilities of aluminum ions in Ni_2P and Cu_3P were studied [90,91]. They demonstrated that incorporation of Al^{3+} into Ni_2P can generate Al_mNi_nP and elemental Ni [90]. Further, compositing with reduced graphene oxide was applied to improve the capacity and cycling stability of Ni_2P in AIB [91]. Moreover, elemental halogen has been applied as cathode in I_2|Al battery, where the reaction between Al and I_2 lead to a thin AlI_3 layer formed [92–94]. This reaction can proceed in wide range of electrolytes, including non-aqueous electrolyte, ionic liquid, solid state electrolyte, and even aqueous electrolyte. Recently synthesized polyvinylpyrrolidone-active carbon composite possessed the hydrogen bonding between PVP and iodine, guaranteeing depression of the shuttle effect of polyiodide and lengthening the cycle life [94].

2.4.6. Drawbacks with RTIL

Some drawbacks are worth noting when using RTILs. One may arise from the air and moisture sensitivities of ILs. The reaction or corrosion of ILs with other battery components (e.g., stainless current collector and the polymer binders, such as polyvinylidene difluoride (PVDF)) are being continuously assessed [60,95]. There is a drive to produce novel ILs via approaches from chloride substitution and immobilization against moisture [3]. Further, electrochemical windows of the chloroaluminate type ILs are generally ≤2.4V, which limits the output voltage of the positive electrode [3]. The side reaction of chloroaluminate-based ILs can not be ignored, such as oxidation of $AlCl_4^-$ to give toxic Cl_2. The relatively high cost of ILs can also impede the AIB fabrication. Concerning this, urea eutectic system and NaCl system have been developed. Decomposition and dissolution of the cathode materials in chloroaluminate-based ILs were known, where this instability can cause uncontrollable “shuttle effect” [76].

Critically, Al dendrite growth has been reported when using ILs, especially under high current density [60]. The native surface Al_2O_3 layer played an effective role on restricting the growth of Al dendrites, where removal of this surficial layer can lead to disintegration of Al anode [96]. The underlying mechanism of how ILs immerse through the dense, uniform, but nonionic-conducting layer to react with beneath Al metal, was proposed to the defects in the surface Al_2O_3 layer facilitating infiltration of ILs and then Al stripping/plating with possible dendrite formation. It was found that the non-corrosive Al(OTF)$_3$/[BMIm]OTF IL was not able to remove the surface Al_2O_3 layer from Al metal [97]. Due to the compact nature of the surface oxide layer, no stripping/plating activity was observed unless Al metal was pretreated (e.g., in $AlCl_3$/[EMIm]Cl). It was believed that the highly corrosive $Al_2Cl_7^-$ was responsible for the partial etching of the oxide film, where the resulted film played a dual role of allowing Al stripping/plating and inhibiting Al dendrite formation [98]. Above study on the chemistry of Al in ILs suggests achieving reversible Al stripping/plating via pretreatment.

2.5. Recent development of rechargeable AAIB

In early assessment of the potential cathode candidates for AAIB, three electrode set-up were widely applied with either Pt or carbon materials as the counter electrode, where the applied electrolytes were in salt-in-water regime. As an important class of cathode materials for AAIB, anatase TiO_2 was firstly verified by Liu et al. to accommodate reversible Al^{3+} insertion/extraction in a free-standing TiO_2|1 M $AlCl_3$|graphite three electrode cell with reference to saturated calomel electrode (SCE) (Fig. 5a) [56]. This cell delivered a capacity of 75 mAh g^{-1} at 4 mA cm^{-2} with a discharging plateau at ~(−)0.95 V (Fig. 5c). A pair of redox peaks at −1.26 and −0.84 V (v.s. SCE) was identified to be reversible insertion/extraction of aluminum ion (Fig. 5b). XPS on the surface state of the TiO_2 after aluminum ion insertion revealed the co-presence of Al^{3+} and Ti^{3+}. The later was attributed to charge compensation, where the redox at Ti^{4+}/Ti^{3+} was responsible for the capacity during aluminum insertion/extraction. Later, the roles of anions drew attention in aqueous solutions of aluminum salts. Cl^- ions were revealed indispensable for the effective insertion of Al^{3+} into anatase TiO_2 in aqueous environment, comparing to SO_4^{2-} (Fig. 5d).[55]Synergistic effect of Cl^- and Al^{3+} was proposed, with surface analysis indicating no chlorine-complex formed on Al^{3+} inserted TiO_2 [55]. Since aqueous solutions of aluminum salts present concentration-dependent weak acidic or acidic pH values, it is essential to decouple the effects of coexisting H^+ and Al^{3+} on Al^{3+} intercalation/extraction. A systematic study on acidity revealed that at low pH of ~1, intercalation/extraction of H^+ was the dominant electrochemical process (Fig. 5e) [99]. XPS analysis further confirmed the dominant process by H^+ and unveiled the tendency of H^+ to form hydroxylate on cathode surface that may lead to the steric hindrance effect as reflected in the interfacial Faradaic resistance. To enhance the performance of TiO_2 based AAIB, strategies like reducing TiO_2 particle size and incorporating conducting components were employed. TiO_2 nanospheres of ~15 nm and ~180 m^2 g^{-1} (~3.5 higher surface area than commercial counterparts) endowed the TiO_2 nanosphere|1 M $AlCl_3$|Pt cell with the advantages of smaller voltage difference between redox pairs, much improved discharge capacities of 183, 126, and 108 mAh g^{-1} at 0.15, 1.5, and 6 C comparing to its commercial counterparts, and good rate performance and cycle stability (Fig. 5f) [100]. The merits were attributed to its porous structure with high surface area, and consequently the high electrode/electrolyte contact area. By adding graphene to increase the conductivity of anatase TiO_2, its Al^{3+} ion storage capability was also found to be much improved due to highly enhanced diffusion coefficient of Al^{3+} [57].

Besides TiO_2, open framework PBA copper hexacyanoferrate nanoparticles were also investigated in aqueous $Al_2(SO_4)_3$ electrolyte [88]. With its rationalized tunnel size, successful Al^{3+} insertion indicates possible desolvation process of hydrated Al^{3+} at solid-electrolyte interface. Interestingly, copper hexacyanoferrate nanoparticles showed higher capacity and longer cycling stability in aqueous electrolyte than those in organic electrolyte [67,68].

Based on above, an electrolyte allowing reversible Al stripping/plating is key to developing AAIB with Al metal anode. A detailed discussion on recent development of electrolytes for aqueous metal ion battery can be referred to our recent review [19]. With proper electrolyte, it is thrilling to explore high performance cathode material with reaction mechanistic study.

Wu et al. applied 5 M aluminum trifluoromethanesulfonate (Al(OTF)$_3$) aqueous solution as the electrolyte for the long-term focused cathode material MnO_2 (Fig. 3d) [11]. This electrolyte showed a potential window of ~(−)0.3–3.3 V w.r.t. Al^{3+}/Al, which is advantageous comparing to other aqueous aluminum electrolytes (Fig. 2c). Based on this, a 200 h galvanostatic charge/discharge profile was demonstrated. $Al_xMnO_2{\cdot}nH_2O$|Al(OTF)$_3$-H_2O|Al was then assembled, where reversible ex/insertion of Al^{3+} was claimed. Layered $A_xMnO_2{\cdot}nH_2O$ was transferred from spinel Mn_3O_4 by charging to 1.8 V (vs. Al/Al^{3+}) at 30 mAh g^{-1}. The resulted $Al_xMnO_2{\cdot}nH_2O$ possessed a high operation voltage to

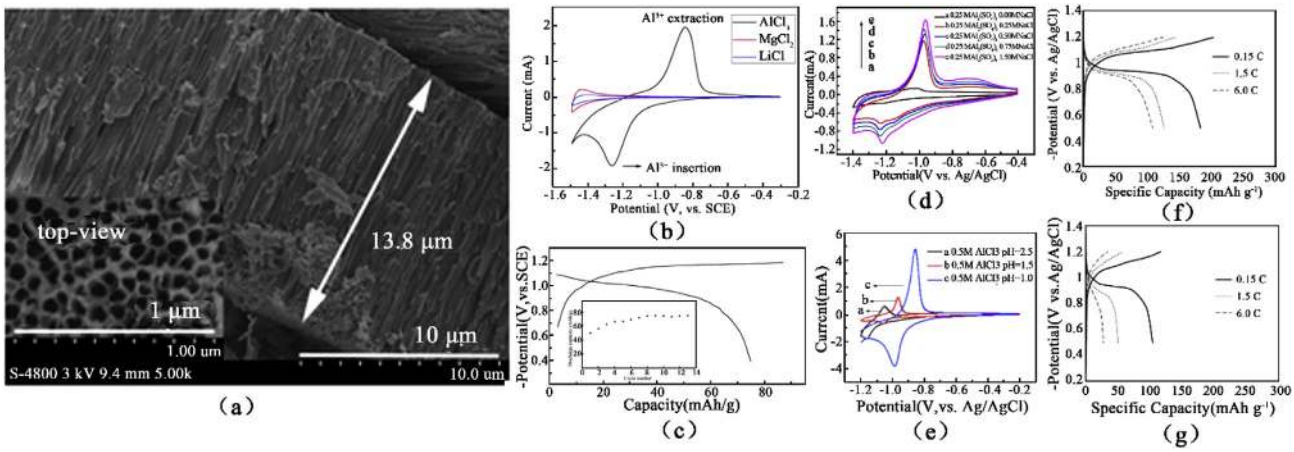

Fig. 5. (a) SEM of arrays of anatase TiO_2 nanotubes, with (b) its CV at 20 mV s^{-1} and (c) typical charge/discharge profile in the 13th cycle at 4 mA cm^{-2}, in 1 M $AlCl_3$ aqueous solution [56]. CVs of the arrays of anatase TiO_2 nanotubes in (d) 0.25 M $Al_2(SO_4)_3$ mixed with a series of NaCl aqueous solutions [55] and (e) 0.5 M $AlCl_3$ with a series of pH values [99]. (f, g) Comparison on initial charge/discharge curves of TiO_2 nanospheres and their commercial counterparts at different rates [100]. (a–c) Reproduced with permission [56]. Copyright 2012. Royal Chemical Society. (d) Reproduced with permission [55]. Copyright 2014. Elsevier. (e) Reproduced with permission [99]. Copyright 2016. Elsevier. (f, g) Reproduced with permission [100]. Copyright 2017. Elsevier.

accommodate Al^{3+} ions at ~1.2 V, where aqueous electrolyte and crystal water was believed to shield the electrostatic interaction between Al^{3+} and host frameworks, and delivered a high specific capacity of 467 mAh g^{-1} at 30 mA g^{-1} with discharge plateaus at ~1.2 and ~0.8 V. At ~65 cycles, the capacity can still retain at ~270 mAh g^{-1}. The insertion of Al^{3+} was verified by the elemental study. Blue shift of binding energies of $Mn2p^{3/2}$ and $Mn2p^{1/2}$ indicates Mn(IV) in MnO_2, together with a 75.0 eV binding energy for Al^{3+} that possibly engages into the host structure. First-principle calculations reveals the spinel-to-layer transition is initiated by dissolution of Mn^{2+} in the tetrahedral sites, followed by competition between water molecular and charge carrier to form the inserted phase AMn_2O_4 (A = H_2O, Li^+, Na^+, and Al^{3+}), where $Al_xMn_2O_4$ is the most thermodynamically favored phase comparing to birnessite structure and insertion of water molecules (Fig. 6a). It is worth noting that the reported spinel-to-layer transition is the reverse to the known spontaneous layer-to-spinel transfer which originates from the migration of Mn and leads to capacity loss. The dominant charging process was proposed as:

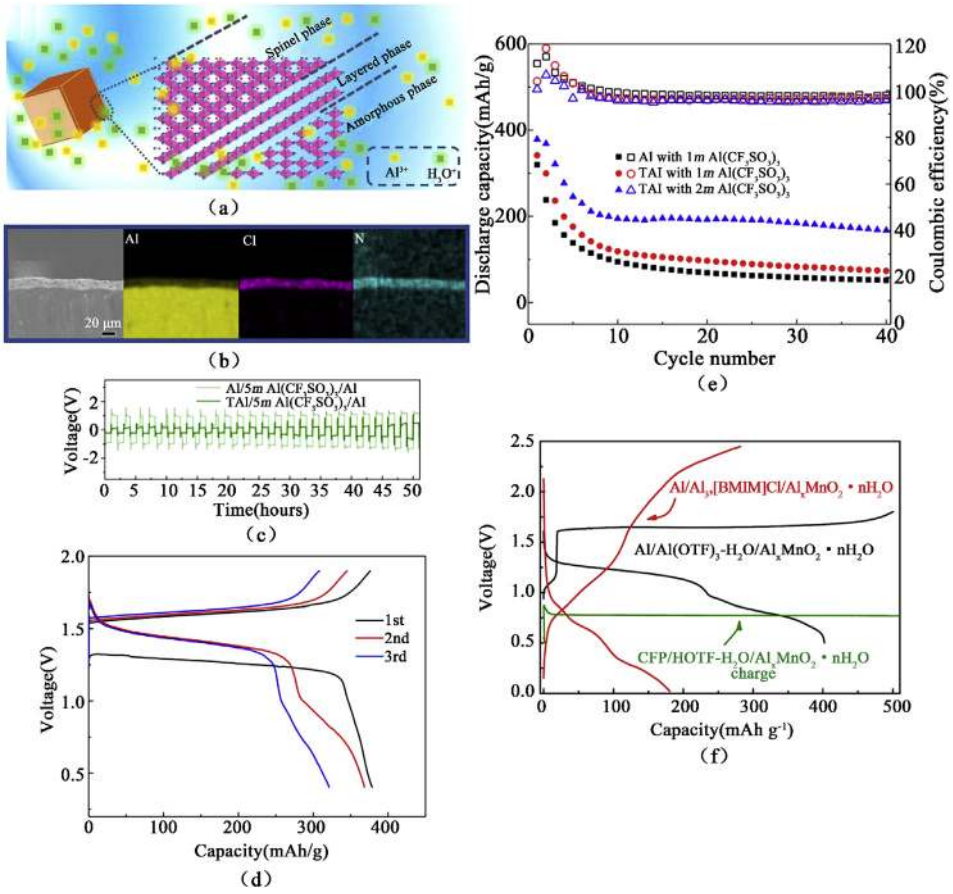

Fig. 6. (a) Schematic showing of the structure change of $Al_xMnO_2{\cdot}nH_2O$ [11]. (b) Typical charge/discharge curves of the MnO_2|Al cells with different electrolytes. (Ref) (c) Cross-sectional SEM image of a TAl foil and corresponding EDX mapping of Al, Cl, and N. (d) Stripping/plating using Al|Al and TAl|TAl cells with 5 M $Al(CF_3SO_3)_3$ aqueous electrolyte [10]. (e) Charge/discharge curve of the MnO_2|2 M $Al(OTF)_3$|TAl cell at 100 mA g^{-1}, with (f) Cycling performance using Al or TAl and in 1 M or 2 M $Al(OTF)_3$ [10]. (a,b) Reproduced with permission [11]. Copyright 2019. Springer Nature. (c–f) Reproduced with permission [10]. Copyright 2018. American association for the advancement of science.

$$Al_yMnO_2{\cdot}nH_2O - 3(y\text{-}x)e \rightarrow Al_xMnO_2{\cdot}nH_2O + (y\text{-}x)Al^{3+} \quad (15)$$

5 M $Al(OTF)_3$ was also applied to a PBA $Fe[Fe(CN)_6]$ cathode [101]. In the $Fe[Fe(CN)_6]$|5 M $Al(OTF)_3$|activated carbon three-electrode setup, its discharge capacity increased to ~116 mAh g^{-1} after two cycles with discharge plateaus at ~0.8, 0.5, and −0.1 V v.s. Ag/AgCl, which is close to its theoretical capacity of 119 mAh g^{-1}. Also, it shows the efficient depression of oxygen evolution reaction and hydrogen evolution reaction and dissolution of cathode materials.

More than electrolyte, SEI on Al can serve as a platform to build AAIB. In a pioneering report by Zhao et al., an IL-enriched film was found constructing the interface, which can simultaneously erode the Al_2O_3 film and protect the Al metal against subsequent formation of the oxide [10]. Importantly, this interphase was transferrable that endowed the treated electrode with exceptional reversibility in Al stripping/plating (Fig. 6c and d). The electrolyte used to form SEI was $AlCl_3$/[EMIm]Cl with the ratio of 1.3:1. Al anode was polished till shinny surface with metallic luster, which was then impregnated in the IL to form the SEI (the anode was then denoted as TAl). Surface analysis, especially XPS and ATR-FTIR, revealed an Al salt dominated on the surface, which was likely $AlCl_3$ with the presence of imidazole ions. Comparison on stripping/-plating in $Al_2(SO_4)_3$ and $Al(OTF)_3$ with a series of molar concentrations indicates the much reduced charge transfer resistance when applying TAl, especially at higher electrolyte concentration. In terms of polarization during stripping/plating, TAI showed an order of magnitude lower value comparing to Al in both electrolytes, though the polarization of TAI|TAI increased with increasing concentration of both electrolytes. Hence, this artificial SEI demonstrates promising functions of preventing oxidation of Al, providing an acidic environment that stabilizes SEI, maintaining a fresh Al, and enabling the operation of cells.

TAI was successfully applied in MnO_2|$Al(OTF)_3$|TAI rechargeable AAIB with aqueous electrolytes, e.g., 2 M $Al(OTF)_3$. An average discharge potential of ~1.3 V was obtained with corresponding capacity of 380 mAh g^{-1}, energy density ~500 W h/kg, and a practical estimation of ~235 W h/kg (Fig. 6e and f). During discharge, the peaks of MnO_2 remained suggesting Al^{3+} or Al^{3+} based complex ion was not incorporated into the lattice of MnO_2. Interestingly, new phase was observed at cathode, where the diffraction peaks can not be assigned to any known Mn-based product, and turned out to be water soluble. It was uncovered to be a compact and smooth coating on MnO_2 nanorods, which disappeared upon charging. Elemental study indicated the Al-rich nature of this water soluble discharge product, and presence of low-valence Mn material (most likely Mn_3O_4). Overall reaction mechanism was further proposed:

$$Al + xMnO_2 + (3/2 + z)H_2O + [ele] \leftrightarrow yMnO_{(2\text{-}3/2y)}@(x\text{-}y)MnO_2 + Al(O\text{-}H)_3[ele]zH_2O \quad (16)$$

This method was further applied to a MnO_2|$Al(OTF)_3$+$MnSO_4$|TAl cell, where the addition of Mn^{2+} salt was employed to enhance the cell performance [59]. Pre-addition of 0.5 M $MnSO_4$ into the 2 M $Al(OTF)_3$ increased the second discharge capacity to 554 mAh g^{-1} at 100 mA g^{-1}, compared with 350 mAh g^{-1} with only $Al(OTF)_3$, which lead to a boost of energy density to 620 W h kg^{-1}. Meanwhile, the cycling stability was greatly improved, where the cell with 0.5 M $MnSO_4$ maintained a capacity ~320 mAh g^{-1} at 65th cycle, comparing to ~40 mAh g^{-1} at 30th cycle for the cell with only $Al(OTF)_3$. The advantage of introducing Mn^{2+} in the electrolyte was attributed to the shifting of reaction balance towards forming $Al_xMn_{(1\text{-}x)}O_2$, which was the effective reversible cathode material after 1st charging process.

In addition, water-in-salt formulation based on $AlCl_3{\cdot}6H_2O$ has been applied to a customized graphite|$AlCl_3$|Al cell [102]. This formulation managed to lower the onset potential of hydrogen evolution reaction to ~(−)2.3 V (v.s. Ag/AgCl), which allowed successful deposition of metallic Al. In this battery system, dual ions of $AlCl_4^-$ and Al^{3+} operated during the reversible charge storage process.

From above developed approaches, utilizing Al metal anode becomes one exciting breakthrough in AAIB. Specifically, Table 4 lists current AAIBs using Al metal anode.

3. Challenges

Till now, AIB is the most-studied triple-electron-transfer battery system. Though with notable breakthroughs recently, problems and drawbacks remain for AIBs. Further in aqueous system, challenges lie in both transferring the established methods or technologies to AAIB and dealing with a whole range of arising issues from this different electrochemical system. Hence, fundamental research on novel electrolytes, the electrolyte-electrode interface (including solid-electrolyte interfaces) and the bulk electrode behavior are vital (Fig. 7).

3.1. Electrolyte

To develop an electrolyte for AIBs, the following factors need to be considered, which is applicable to electrolyte for AAIBs: (1) a suitable electrochemical window for enabling battery cycling with minimal side reactions; (2) a high ionic conductivity but low electron conductivity; (3) equilibria interactions between solute ions and solvent molecules where a suitable activation energy for solvation/desolvation is preferred; (4) the electrolyte-electrode interface, where a possible SEI can be beneficial to the electrode; (5) corrosion effects leading to uncontrolled dissolution of electrodes, e.g., low pH conditions at which certain metal oxides dissolve; and (6) compatibility/inertness towards auxiliary components of the battery, such as the binder for the electrode material and the battery casing.

A few functioning electrolytes has been reported for AAIB so far, primarily based on investigation on $AlCl_3$ based electrolytes and recent exploration of $Al(OTF)_3$ solution. This highlights that electrolyte is one of the major obstacles for AAIB development. Water-in-salt electrolytes have been successfully applied in aqueous LIB, NIB, and ZIB, where the formulations expand the potential window, reconfigure the cation coordination environment, alter the solvation-desolvation process at SEI, facilitate ion transport, and hence favor the reversible stripping/plating of metal anode [4,104–106]. But limited solubility of $Al(OTF)_3$ is an intrinsic constraint to obtain an analogue water-in-salt electrolyte for Al electrochemistry. Hybrid salts, e.g., 1 M $Zn(TFSI)_2$+20 M LiTFSI (TFSI, bis(trifluoromethanesulfonyl)imide), can be an option to form water--in-salt electrolyte for AAIB [107]. Besides, inorganic-based molten salts can be choices [102,108–110].

On the other hand, quasi-solid state electrolyte/solid state electrolyte may also be a practical solution to implementing AAIB by widening the potential window and retaining moderate ion conductivity. A ionic-liquid-based polymer electrolyte has been developed consisting of polyethylene oxide, SiO_2, $AlCl_3$, and 1-ethyl-3-methylimidazolium bis(-fluorosulfonyl)imide ([EMIm]FSI) [111]. For this electrolyte, an electrochemical window of 3V (vs. Al^{3+}/Al) was reported with an ionic conductivity of 0.96 mS/cm. However, there were no redox features of stripping/plating found in the CV curve, which suggests that the oxygen containing group (e.g., ether) might alter the coordination of $Al_2Cl_7^-$ thus reducing the electrochemical activity. Hence, selection and synthesis of constituents in the quasi solid-state electrolyte offer large room for AAIB development.

Moreover, identifying the mobile species in the electrolyte for AIB can be tricky. The ambiguity on how $Al_2(WO_4)_3$ batteries work is a typical example for such issue in solid-state electrolytes [6]. Whereas the coordination environment of cations is reshaped in water-in-salt electrolytes from its salt-in-water counterparts [107,112], it is believed that the solvation-sheath structure can be further modulated by using asymmetric salt formulations [113,114]. Consequently, resolving the mobile species in the electrolyte presents a peculiarly interesting problem for current AAIB research.

Table 4
Electrochemical performance of AAIB cells with Al metal anode.

Cathode	Anode	Electrolyte	Discharge voltage	Capacity /Current	Rate/Current	Retention (% at cycles)	Ref.
MnO_2	$AlCl_3$/[EMIm]Cl treated Al	2 M $Al(OTF)_3$	~1.3 V	380 mAh g^{-1} /0.1 A g^{-1}	~100 mAh g^{-1} /0.5 A g^{-1}	~44% at 40	[10]
MnO_2	$AlCl_3$/[EMIm]Cl treated Al	2 M $Al(OTF)_3$ + 0.5 M $MnSO_4$	~1.35 V	530 mAh g^{-1} /0.1 A g^{-1}	125 mAh g^{-1} /0.3 A g^{-1}	~60% at 65	[103]
$Al_xMnO_2{\cdot}nH_2O$	Al	5 M $Al(OTF)_3$	~1.2 V	467 mAh g^{-1} /0.03 A g^{-1}	–	58% at 50	[11]
graphite	Al	$Alcl_3{\cdot}6H_2O$ based "water-in-salt" electrolyte	average 1.4 V	165 mAh g^{-1} /0.5 A g^{-1}	–	99% at 1000	[102]

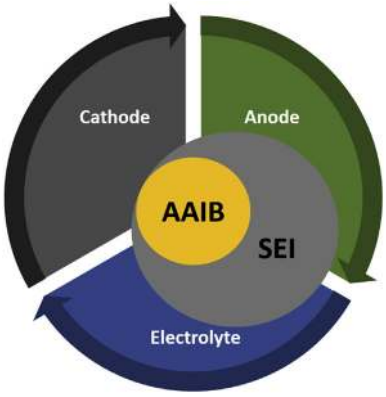

Fig. 7. Key components of AAIB urging in-depth study.

3.2. Pursuing reversible stripping/plating of Al

Critically, the electrochemical behavior of Al metal in an electrolyte determines the feasibility of the designed battery cell. Note that previous AAIB design mostly applies three electrode setups using Pt or graphite as the counter electrode. Hence, to evaluate the feasibility of using Al metal anode, details on the behavior of metallic Al with currently applied electrolytes warrant in-depth survey. It is always desirable to observe a reversible metallic stripping/plating characteristic in the CV for reported battery systems. Additionally, decoupling the first few cycles of galvanostatic charge/discharge profiles can be attempted [115], which may help to establish a more solid understanding on Al stripping/plating. More stable charge/discharge voltage profile over long-term cycling needs be pursued. A practical question on developed electrolyte systems could be the failure mechanism, which causes Al|Al symmetric cells to cease being reversible over time. Passivation might be a possible cause, e.g., instinctively from CV with 5 M $Al(OTF)_3$ aqueous solutions. On a system-to-system basis however, further information on the Al anode for full cells have been rarely discussed so far to provide a clear picture.

To pursue reversible Al stripping/plating, fundamental properties of Al metal and the surface aluminum oxide layer have been extensively studied. The correlation between the electrochemical properties and the battery performance of polycrystalline Al, Al (001), Al (110), and Al (111) single crystals in alkaline electrolyte has revealed that Al (001) displayed lower corrosion rate and higher capacity density due to the lower surface energy [116]. Further, in the early development of MnO_2|Al primary batteries, the addition of Zn, Cd, Mg, or Ba to the Al anode led to an increase in the anode potential by ~0.1–0.3 V, while the addition of Ga, Hg, Sn, or In led to an increase in the anode potential by ~0.3–0.9V [8]. Also, alloying modification of aluminum in an attempt to alter the oxide layer has been explored in alkaline electrolytes, using doping elements such as Ga, In, Sn, Zn, Mg, Ca, Pb, Hg, Mn, and Tl [8]. Notwithstanding alkaline systems, the role of a thin and uniform aluminum oxide layer in $AlCl_3$/[EMIm]Cl has likewise been revealed to restrict the growth of crystalline aluminum dendrites and be effective against surface corrosion, which then successfully operated an Al|graphene cell [96]. Evidently, research on RTILs provides key insights to Al stripping/plating [117,118]. Above mentioned methods and technologies in non-aqueous systems, i.e., Al with specific crystallographic planes, alloys of Al, and designed surface layer, have not yet been verified in the currently emerging aqueous systems. And the corresponding database works as cornerstone to achieve reversible stripping/plating of Al. Further, it remains unknown for any possible Al dendrite formation in the aqueous system.

3.3. SEI for Al metal

Different from dilute aqueous electrolytes, SEI in water-in-salt electrolyte may receive contributions from reduction of both anion species and dissolved oxygen [119,120]. In 21 M LiTFSI systems, the SEI consists of LiF and Li_2O(inner)-Li_2CO_3(outer), which chemically-complexes with the anode surface. When an additive tris(trimethylsilyl) borate is employed in 21 M LiTFSI, an amorphous layer forms consisting of $Si(OH)_x$ and $B(OH)_3$ which improves the cycling stability of $LiCoO_2$|Mo_6S_8 cells [121].

On the other hand, we have recently unambiguously identified the presence of layer hydroxides on metal anodes in aqueous ZIBs [122]. This effective SEI was proposed to form via precipitation. Here, planar morphology of the SEI can be manipulated through functional groups from the polymeric membrane, promoting long life-cycle of stripping/plating. The role of this layer-hydroxide SEI on cathode materials has also been discussed [123–125]. To induce a SEI, great potential can be explored for polymeric membrane or polymeric electrolyte across different battery systems [126–128]. But an open and key question remains whether any effective SEI can form in AAIB, competing against the favored formation of aluminum oxide, especially for newly developed electrolytes.

Indeed, artificial SEIs are being developed continuously for rechargeable batteries [129,130]. Graphene film of 1–50 nm when applied on $LiMn_2O_4$ via Langmuir trough-based technique significantly enhanced the cycling performance of an aqueous $LiMn_2O_4$|Zn cell [131]. The graphene film was shown to suppress both the oxidation of carbon additive in the cathode and the Jahn-Teller distortion. Besides deposited carbon materials on anode, artificial SEI can also be formed from the decomposition of organic solvents. For example, a Mg^{2+}-conducting interface on Mg anode was thermal cyclized from polyacrylonitrile and $Mg(OTF)_2$ [132]. With this SEI, reversible Mg stripping/plating was achieved in nitrile or carbonate electrolyte, where direct reaction between Mg and electrolytes seemed to be inhibited. The SEI facilitated the V_2O_5|Mg cell in 0.5 M $Mg(OTFI)_2$ in PC and 3 M H_2O, where water is known to passivate Mg surface and to break the reversible Mg chemistry.

Artificial SEI on Al through $AlCl_3$/[EMIm]Cl exhibited advances on operational rechargeable AAIB [10]. Based on Section 2.(iv)(F) and 2.(v), it could be resulted by competing etching of the surface Al_2O_3 layer and depositing of aluminum complex on Al metal via the IL. It would be interesting to gain the structural information of this ~10–20 μm SEI,

which may allow generalizing this method among options of interaction/complexation towards SEI for Al metal anode. There is a lack of reports on the stability of this kind of SEI in either air or aqueous electrolyte. Also, little is known during evolution of the SEI with increasing electrolyte concentration or current density. Changing polarization profiles reflects evolving interface. Especially, it might be fundamentally important to assess the competing effects from highly concentrated anions (e.g., OTF^-) in the electrolyte with imidazole or even $AlCl_3$. This is important given that above 3 M $Al(OTF)_3$, both increasing magnitude and changing profile of polarization suggest complex interaction on TAl. Moreover, SEI may be more complex on the cathode side, e.g. in MnO_2-|$Al(OTF)_3$|TAl, as discussed earlier.

In short, the formation of SEI is intrinsically related to the electrolyte system, which is likely more complex in water-in-salt electrolyte or highly concentrated electrolyte. Artificial SEI may be produced from a synthetic route separately from the applied electrolyte, but the question that tantalizingly remains is how to form one which suits rechargeable AAIBs.

3.4. Cathode materials

To study the cathode materials for AAIB, lessons from cathodes for AIB are considered first. One of the major obstacles is the difficulty to extract Al^{3+} from the host once inserted, due to the strong electrostatic interaction of Al^{3+} with the host lattices. This results in irreversible volume expansions, poor structural reversibility and potentially the need for acidic conditions to push the Al^{3+} ions out, but which inadvertently also dissolves the cathode structure. Also, relatively low discharging voltage plateaus limit achieving high energy densities. And the fact that cathodes are unable to deliver their theoretical voltages and capacities indicates the complicated mechanism of Al^{3+} insertion with possible high overpotentials [3].

Discussion on cathode candidates in aqueous ZIB and AAIB can be found in recent reviews [3,12,13,133]. General problems for multivalent cations are specifically outlined here: (1) limited mobilities of MV cations within host-structure lattices due to their high charge-to-radius ratio, where crystal structures are preferred with no pre-existing MV ion occupancies, ion-migration pathways allowing minimal coordination change between different states for MV ion, and reducing repulsion between MV ion and transition metal centers in the host [134]; (2) limited cycling stability of electrodes, where Al doping was found to improve the structural stability [135,136]; (3) proton/hydronium co-insertion; (4) uncontrolled dissolution of redox-active transition-metal components, which is closely related their stable potentials in the designed reaction system; and (5) O_2-driven parasitic reactions from dissolved O_2 in the electrolyte, where suppressing oxygen evolution reduction at electrode needs to considered. Though transition metal oxides have been intensively investigated for aqueous ZIB in recent years [137,138], whether analogous mechanisms and performances can be achieved in AAIB still remains as an open question.

Study on TiO_2 based AAIB highlights the significance of nanostructure in pursuing high performance. The synthesized layer, porous, and hollow structure benefit surface/interface area, ion transportation across the interface, and the kinetics of the electrochemical reactions. Also, defect engineering can be anther potential route. For example, Koketsu et al. demonstrated that introducing cationic vacancies unlocked the electrochemical activity of anatase TiO_2 towards MV cations [58]. This design is based on that in stoichiometric anatase TiO_2, thermodynamic driving force for the intercalation of MV ions at an interstitial site is smaller than that for Li^+. After introducing vacancies, TiO_2 showed ~4 times improvement in discharge capacity than the pristine one with $AlCl_3$/[EMIm]Cl. It will be promising that these design concerns are implemented for AAIB.

In aqueous rechargeable batteries, the interplay between water, proton (H^+), and hydronium ($H(H_2O)_n)^+$) may open new routes for developing AAIB. The competing effects of partial screening of the MV cation by water molecule and diffusion barrier by a high number of protons/hydronium for intercalating cations have been recognized [5,139]. Water molecule benefits structure stability and high capacity and rate capability, e.g., in Zn^{2+}/H_2O pillared layered V_2O_5 [140]. Besides stabilizing host structure via strong hydrogen bonding, crystal water may favor the transfer of partially hydrated MV cations across the solid-liquid interface [141–143]. The role of H^+ can be clearly distinguished between α-MnO_2|Zn cells with or without H_2O in organic electrolyte [144]. Insertion of both H^+ and Zn^{2+} coexists in the ε-MnO_2|$ZnSO_4$|Zn cell, as featured by distinct sloping plateaus, where thermal gravimetric analysis suggests it is the proton that functions than hydronium [145]. For AAIB, co-insertion of H^+ and Al^{3+} has been identified in the TiO_2|$AlCl_3$|Pt, where H^+ played a dominant role [99]. However, in the recent Al_xM-nO_2·nH_2O|$Al(OTF)_3$-H_2O|Al cell, contribution from hydronium to the capacity was ruled out, and Al^{3+} intercalation/extraction was the dominant charge storage process (Fig. 6b) [11]. On the other hand, hydronium is believed to induce a spinel-to-layer transition for Mn_3O_4 [146]. The interplay between water, proton, and hydronium is complex. Discrepancy on the effects of H^+ and H_3O^+ in different electrolytes for AAIB suggests system-varying Al^{3+} charge storage mechanism. It is fundamentally important to distinguish the roles of H^+ and $(H_2O)_n^+$ during Al^{3+} insertion/extraction. Approaches to manipulate the effects of water, proton, and hydronium on active material include adjusting pH, forming supersaturated salt or water-in-salt, and designing proper crystal structure [147–149].

Meanwhile, exploring new cathode materials for AAIB is on its way, e.g., MoO_3 [150]. The family of vanadates has been proposed, e.g., $AlVO_3$ and $FeVO_4$ [151,152]. Metal halides, including $NiCl_2$, CuF_2, and $FeCl_3$, have been reported to react with Al^{3+} [153]. It is still unknown whether metal halides can be candidates for AAIB in water-in-salt electrolyte or quasi-solid state electrolyte. Also, elemental halogen has shown its electrochemical activity in I_2–C|KI aqueous solution|Al and C|KI + I_2 aqueous solution|C cells, exhibiting discharging plateaus of ~0.6–0.7 V [93]. It is promising that Al^{3+} ions are the active species in the reaction and meantime interesting to survey long-term cycling provided that AlI_3 is water soluble. Nevertheless, emerging cathode materials urge employing advanced characterization tools for mechanistic studies.

4. Outlook

Research on the aluminum ion battery is currently experiencing a worldwide pursuit. Though rechargeable AIBs have been developed with promising performance, fundamental study is essential to overcome the slow kinetics, inferior cycling stability, and compatibility issues between metallic Al and currently available ILs. Compared with traditional AIB, AAIB is now at its nascent stage with great potential on power density and energy density metrics among all types of aqueous ion batteries (Fig. 8). Facing the great challenge of reversible Al stripping/plating, pursuing novel aluminum electrolyte systems may synergistically open more opportunities towards understanding and applying aluminum chemistry/electrochemistry.

For electrolyte, an ideal formulation is able to allow reversible Al stripping/plating and most importantly control the formation of the Al_2O_3 passivation layer. Water-in-salt electrolytes, quasi-solid state electrolytes, and deep eutectic solvents are proven choices for widening the electrochemical potential window by the suppressing hydrogen evolution reaction. Simultaneously however, the extent of corrosive properties imparted by electrolyte liquids cannot be ignored.

For Al metal anode, some basic information are useful or even essential for a reported electrolyte: (1) CV showing Al stripping/plating; (2) decoupled presentation of the voltage profiles for the first few cycles, which may indicate the possible formation of electrode-electrolyte interface; and (3) demonstration of long term cycle-life, or alternatively, possible failure mechanisms. An intense research pursuit in the coming years could be constructing an artificial SEI layer on Al metal while competing against the Al_2O_3 passivation layer. Endeavors on developing

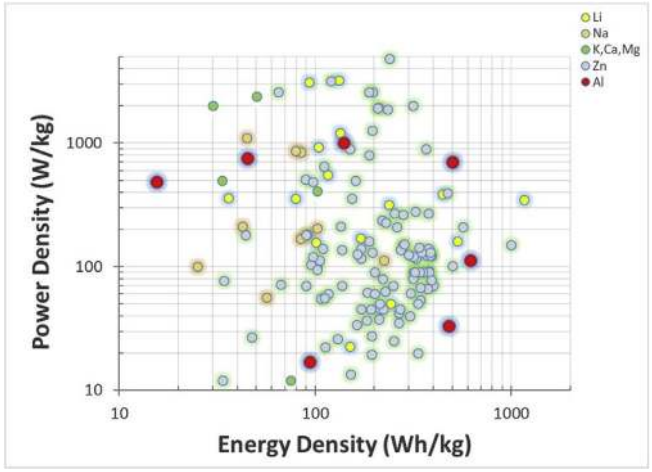

Fig. 8. Summary of energy densities and power densities of the representatives of aqueous ion batteries.

above strategies will probably be highlighted by copious publications on aluminum chemistry/electrochemistry.

For the cathode materials, though considerable research activities have been done to explore advanced cathode materials for AIB, few of them may be suitable for AAIB. The following aspects may be worth studying for cathodes in AAIB: (1) expanding the crystallographic interlayer distance in layer-structured materials to weaken electrostatic interactions and therefore decrease the ionic diffusion energy barrier for fast accommodation of more Al^{3+} ions; (2) exploring other variants of layer-structured or tunnel-structured materials possessing crystallographic water for shielding the active charge of trivalent Al^{3+} ions as the ions ease through the structure; (3) designing nanosized/3D cathode structures with large surface areas, porosity, and exposed highly active facets to improve both capacitive contribution and battery kinetics; (4) creating mixed-valence chemistries and vacancy sites to optimize the ion transfer tunnel and increase ionic conductivity; (5) compositing with highly-conductive carbons to elevate the performance of oxides, sulfides or other materials; (6) investigating polyanion cathodes to push up the operating discharge potential. Moreover, advanced characterization techniques combined with theoretical studies are key to accelerate the development of AAIBs.

It is important to stress that the role of water will be continuously explored in AIB or AAIB. Water may come into play in three cases: (1) involved in the crystal structure of the electrode active material influencing both intercalation and conversion reactions; (2) as part of the hydration shell of the Al^{3+} ions; (3) or as part of the electrochemistry occurring at the electrode-electrolyte interface influencing solvation-desolvation behavior of the Al^{3+} ions. More complex scenario may also occur when protons or hydronium ions are participating into the battery chemistry.

Based on the current state of development, some design principles to pursuit better AAIBs with Al metal anodes are proposed, and open to future questioning and updating: (1) a developed electrolyte is able to efficiently conduct Al^{3+}, with sufficiently wide potential window depressing hydrogen evolution reaction and further allowing Al stripping/plating; (2) an agent, like IL, to form a SEI on Al metal is expected to erode the Al_2O_3 surface layer with a controllable degree, and simultaneously interact with aluminum to form a stable SEI/effective SEI layer; (3) an artificial SEI is expected to be stable in the applied electrolyte system, protecting Al metal away from forming a thick and dense Al_2O_3; (4) a cathode material is desirable to have large enough conduction tunnels or interlayer spacings to accommodate Al^{3+}, or even Al^{3+}-based hydrated ions (considering solvation-desolvation kinetics at SEI).

Moreover, the vast availability of aluminum as well as their commercial availability through the aluminum value chain and infrastructure, together with high safety make AIB/AAIB an important post-lithium concept. While achieving exciting progress in performance, sustainability as well as recycling of AIB/AAIB might be taken into serious consideration later.

Acknowledgement

This work was financially supported by the National Research Foundation of Singapore (NRF) Investigatorship Award Number NRFI2017-08/NRF2016NRF-NRFI001-22.

References

[1] J. Muldoon, C.B. Bucur, T. Gregory, Quest for nonaqueous multivalent secondary batteries: magnesium and beyond, Chem. Rev. 114 (2014) 11683–11720.
[2] G.A. Elia, K. Marquardt, K. Hoeppner, S. Fantini, R. Lin, E. Knipping, et al., An overview and future perspectives of aluminum batteries, Adv. Mater. 28 (2016) 7564–7579.
[3] Y. Zhang, S. Liu, Y. Ji, J. Ma, H. Yu, Emerging nonaqueous aluminum-ion batteries: challenges, status, and perspectives, Adv. Mater. 30 (2018) 1706310.
[4] L. Suo, O. Borodin, T. Gao, M. Olguin, J. Ho, X. Fan, et al., "Water-in-salt" electrolyte enables high-voltage aqueous lithium-ion chemistries, Science 350 (2015) 938.
[5] P. Canepa, G. Sai Gautam, D.C. Hannah, R. Malik, M. Liu, K.G. Gallagher, et al., Odyssey of multivalent cathode materials: open questions and future challenges, Chem. Rev. 117 (2017) 4287–4341.
[6] T. Leisegang, F. Meutzner, M. Zschornak, W. Münchgesang, R. Schmid, T. Nestler, et al., The aluminum-ion battery: a sustainable and seminal concept? Front. Chem. (2019) 7.
[7] Z.A. Zafar, S. Imtiaz, R. Razaq, S. Ji, T. Huang, Z. Zhang, et al., Cathode materials for rechargeable aluminum batteries: current status and progress, J. Mater. Chem. 5 (2017) 5646–5660.
[8] Q. Li, N.J. Bjerrum, Aluminum as anode for energy storage and conversion: a review, J. Power Sources 110 (2002) 1–10.
[9] M.-C. Lin, M. Gong, B. Lu, Y. Wu, D.-Y. Wang, M. Guan, et al., An ultrafast rechargeable aluminium-ion battery, Nature 520 (2015) 324.
[10] Q. Zhao, M.J. Zachman, W.I. Al Sadat, J. Zheng, L.F. Kourkoutis, L. Archer, Solid electrolyte interphases for high-energy aqueous aluminum electrochemical cells, Sci. Adv. (2018) 4, eaau8131.
[11] C. Wu, S. Gu, Q. Zhang, Y. Bai, M. Li, Y. Yuan, et al., Electrochemically activated spinel manganese oxide for rechargeable aqueous aluminum battery, Nat. Commun. 10 (2019) 73.
[12] F. Wu, H. Yang, Y. Bai, C. Wu, Paving the path toward reliable cathode materials for aluminum-ion batteries, Adv. Mater. 31 (2019) 1806510.
[13] H. Yang, H. Li, J. Li, Z. Sun, K. He, H.-M. Cheng, et al., The rechargeable aluminum battery: opportunities and challenges, Angew. Chem. Int. Ed. 58 (2019) 11978–11996.
[14] S.K. Das, S. Mahapatra, H. Lahan, Aluminium-ion batteries: developments and challenges, J. Mater. Chem. 5 (2017) 6347–6367.
[15] Y. Ru, S. Zheng, H. Xue, H. Pang, Different positive electrode materials in organic and aqueous systems for aluminium ion batteries, J. Mater. Chem. 7 (2019) 14391–14418.
[16] Y. Liu, Q. Sun, W. Li, K.R. Adair, J. Li, X. Sun, A comprehensive review on recent progress in aluminum–air batteries, Green Energy Environ. 2 (2017) 246–277.
[17] M. Pourbaix, Atlas of Electrochemical Equilibria in Aqueous Solutions vol. 1, Pergamon, Houston, Texas, 1966.
[18] K.A. Persson, B. Waldwick, P. Lazic, G. Ceder, Prediction of solid-aqueous equilibria: scheme to combine first-principles calculations of solids with experimental aqueous states, Phys. Rev. B 85 (2012) 235438.
[19] W. Manalastas Jr., S. Kumar, V. Verma, L. Zhang, D. Yuan, M. Srinivasan, Water in rechargeable multivalent-ion batteries: an Electrochemical pandora's box, ChemSusChem 12 (2019) 379–396.
[20] C. Vargel, Corrosion of Aluminum, Elsevier Science, Oxford, 2004.
[21] E. Deltombe, M. Pourbaix, The electrochemical behavior of aluminum—potential pH diagram of the system AI-H2O at 25 C, Corrosion 14 (1958) 16–20.
[22] S.-T. Myung, Y. Hitoshi, Y.-K. Sun, Electrochemical behavior and passivation of current collectors in lithium-ion batteries, J. Mater. Chem. 21 (2011) 9891–9911.
[23] J. Nakai, T. Miyazaki, On the tunneling current through thin aluminum-oxide films, Jpn. J. Appl. Phys. 3 (1964) 677–686.
[24] R. Shannon, Revised effective ionic radii and systematic studies of interatomic distances in halides and chalcogenides, Acta Crystallogr. A 32 (1976) 751–767.
[25] L.D. Reed, A. Arteaga, E.J. Menke, A combined experimental and computational study of an aluminum triflate/diglyme electrolyte, J. Phys. Chem. B 119 (2015) 12677–12681.
[26] X. Zhang, T.M. Devine, Factors that influence formation of AlF3 passive film on aluminum in Li-ion battery electrolytes with LiPF6, J. Electrochem. Soc. 153 (2006) B375–B383.
[27] Z.J. Karpinski, R.A. Osteryoung, Determination of equilibrium constants for the tetrachloroaluminate ion dissociation in ambient-temperature ionic liquids, Inorg. Chem. 23 (1984) 1491–1494.
[28] K.S. Mohandas, N. Sanil, M. Noel, P. Rodriguez, Electrochemical intercalation of aluminium chloride in graphite in the molten sodium chloroaluminate medium, Carbon 41 (2003) 927–932.

[29] D. Muñoz-Torrero, P. Leung, E. García-Quismondo, E. Ventosa, M. Anderson, J. Palma, et al., Investigation of different anode materials for aluminium rechargeable batteries, J. Power Sources 374 (2018) 77–83.
[30] P.R. Gifford, J.B. Palmisano, An aluminum/chlorine rechargeable cell employing a room temperature molten salt electrolyte, J. Electrochem. Soc. 135 (1988) 650–654.
[31] H. Chen, F. Guo, Y. Liu, T. Huang, B. Zheng, N. Ananth, et al., A defect-free principle for advanced graphene cathode of aluminum-ion battery, Adv. Mater. 29 (2017) 1605958.
[32] L. Zhang, L. Chen, H. Luo, X. Zhou, Z. Liu, Large-sized few-layer graphene enables an ultrafast and long-life aluminum-ion battery, Adv. Energy Mater. 7 (2017) 1700034.
[33] D.-Y. Wang, C.-Y. Wei, M.-C. Lin, C.-J. Pan, H.-L. Chou, H.-A. Chen, et al., Advanced rechargeable aluminium ion battery with a high-quality natural graphite cathode, Nat. Commun. 8 (2017) 14283.
[34] H. Chen, C. Chen, Y. Liu, X. Zhao, N. Ananth, B. Zheng, et al., High-quality graphene microflower design for high-performance Li–S and Al-ion batteries, Adv. Energy Mater. 7 (2017) 1700051.
[35] X. Yu, B. Wang, D. Gong, Z. Xu, B. Lu, Graphene nanoribbons on highly porous 3D graphene for high-capacity and ultrastable Al-ion batteries, Adv. Mater. 29 (2017) 1604118.
[36] H. Chen, H. Xu, S. Wang, T. Huang, J. Xi, S. Cai, et al., Ultrafast all-climate aluminum-graphene battery with quarter-million cycle life, Sci. Adv. (2017) 3, eaao7233.
[37] Y. Wu, M. Gong, M.-C. Lin, C. Yuan, M. Angell, L. Huang, et al., 3D graphitic foams derived from chloroaluminate anion intercalation for ultrafast aluminum-ion battery, Adv. Mater. 28 (2016) 9218–9222.
[38] N.P. Stadie, S. Wang, K.V. Kravchyk, M.V. Kovalenko, Zeolite-templated carbon as an ordered microporous electrode for aluminum batteries, ACS Nano 11 (2017) 1911–1919.
[39] H. Huang, F. Zhou, X. Shi, J. Qin, Z. Zhang, X. Bao, et al., Graphene aerogel derived compact films for ultrafast and high-capacity aluminum ion batteries, Energy Storage Mater. 23 (2019) 664.
[40] J. Smajic, A. Alazmi, N. Batra, T. Palanisamy, D.H. Anjum, P.M.F.J. Costa, Mesoporous reduced graphene oxide as a high capacity cathode for aluminum batteries, Small 14 (2018) 1803584.
[41] C. Zhang, R. He, J. Zhang, Y. Hu, Z. Wang, X. Jin, Amorphous carbon-derived nanosheet-bricked porous graphite as high-performance cathode for aluminum-ion batteries, ACS Appl. Mater. Interfaces 10 (2018) 26510–26516.
[42] Z. Liu, J. Wang, H. Ding, S. Chen, X. Yu, B. Lu, Carbon nanoscrolls for aluminum battery, ACS Nano 12 (2018) 8456–8466.
[43] Y. Hu, S. Debnath, H. Hu, B. Luo, X. Zhu, S. Wang, et al., Unlocking the potential of commercial carbon nanofibers as free-standing positive electrodes for flexible aluminum ion batteries, J. Mater. Chem. 7 (2019) 15123–15130.
[44] J. Tu, J. Wang, S. Li, W.-L. Song, M. Wang, H. Zhu, et al., High-efficiency transformation of amorphous carbon into graphite nanoflakes for stable aluminum-ion battery cathodes, Nanoscale 11 (2019) 12537–12546.
[45] S. Wang, K.V. Kravchyk, F. Krumeich, M.V. Kovalenko, Kish graphite flakes as a cathode material for an aluminum chloride–graphite battery, ACS Appl. Mater. Interfaces 9 (2017) 28478–28485.
[46] H. Sun, W. Wang, Z. Yu, Y. Yuan, S. Wang, S. Jiao, A new aluminium-ion battery with high voltage, high safety and low cost, Chem. Commun. (Camb) 51 (2015) 11892–11895.
[47] X. Zhao, W. Yao, W. Gao, H. Chen, C. Gao, Wet-spun superelastic graphene aerogel millispheres with group effect, Adv. Mater. 29 (2017) 1701482.
[48] J. Jiang, H. Li, J. Huang, K. Li, J. Zeng, Y. Yang, et al., Investigation of the reversible intercalation/deintercalation of Al into the novel Li3VO4@C microsphere composite cathode material for aluminum-ion batteries, ACS Appl. Mater. Interfaces 9 (2017) 28486–28494.
[49] H. Wang, Y. Bai, S. Chen, X. Luo, C. Wu, F. Wu, et al., Binder-free V2O5 cathode for greener rechargeable aluminum battery, ACS Appl. Mater. Interfaces 7 (2015) 80–84.
[50] H. Wang, X. Bi, Y. Bai, C. Wu, S. Gu, S. Chen, et al., Open-structured V2O5·nH2O nanoflakes as highly reversible cathode material for monovalent and multivalent intercalation batteries, Adv. Energy Mater. 7 (2017) 1602720.
[51] D.B. Le, S. Passerini, F. Coustier, J. Guo, T. Soderstrom, B.B. Owens, et al., Intercalation of polyvalent cations into V2O5 aerogels, Chem. Mater. 10 (1998) 682–684.
[52] S. Gu, H. Wang, C. Wu, Y. Bai, H. Li, F. Wu, Confirming reversible Al3+ storage mechanism through intercalation of Al3+ into V2O5 nanowires in a rechargeable aluminum battery, Energy Storage Mater. 6 (2017) 9–17.
[53] W. Wang, B. Jiang, W. Xiong, H. Sun, Z. Lin, L. Hu, et al., A new cathode material for super-valent battery based on aluminium ion intercalation and deintercalation, Sci. Rep. 3 (2013) 3383.
[54] N. Jayaprakash, S.K. Das, L.A. Archer, The rechargeable aluminum-ion battery, Chem. Commun. (Camb) 47 (2011) 12610–12612.
[55] Y. Liu, S. Sang, Q. Wu, Z. Lu, K. Liu, H. Liu, The electrochemical behavior of Cl− assisted Al3+ insertion into titanium dioxide nanotube arrays in aqueous solution for aluminum ion batteries, Electrochim. Acta 143 (2014) 340–346.
[56] S. Liu, J.J. Hu, N.F. Yan, G.L. Pan, G.R. Li, X.P. Gao, Aluminum storage behavior of anatase TiO2 nanotube arrays in aqueous solution for aluminum ion batteries, Energy Environ. Sci. 5 (2012) 9743–9746.
[57] H. Lahan, R. Boruah, A. Hazarika, S.K. Das, Anatase TiO2 as an anode material for rechargeable aqueous aluminum-ion batteries: remarkable graphene induced aluminum ion storage phenomenon, J. Phys. Chem. C 121 (2017) 26241–26249.
[58] T. Koketsu, J. Ma, B.J. Morgan, M. Body, C. Legein, W. Dachraoui, et al., Reversible magnesium and aluminium ions insertion in cation-deficient anatase TiO2, Nat. Mater. 16 (2017) 1142.
[59] S. He, J. Wang, X. Zhang, J. Chen, Z. Wang, T. Yang, et al., A high-energy aqueous aluminum-manganese battery, Adv. Funct. Mater. 29 (2019) 1905228.
[60] L.D. Reed, E. Menke, The roles of V2O5 and stainless steel in rechargeable Al–ion batteries, J. Electrochem. Soc. 160 (2013) A915–A917.
[61] X. Zhang, G. Zhang, S. Wang, S. Li, S. Jiao, Porous CuO microsphere architectures as high-performance cathode materials for aluminum-ion batteries, J. Mater. Chem. 6 (2018) 3084–3090.
[62] J. Wei, W. Chen, D. Chen, K. Yang, Molybdenum oxide as cathode for high voltage rechargeable aluminum ion battery, J. Electrochem. Soc. 164 (2017) A2304–A2309.
[63] W. Kaveevivitchai, A. Huq, S. Wang, M.J. Park, A. Manthiram, Rechargeable aluminum-ion batteries based on an open-tunnel framework, Small 13 (2017) 1701296.
[64] M. Chiku, H. Takeda, S. Matsumura, E. Higuchi, H. Inoue, Amorphous vanadium oxide/carbon composite positive electrode for rechargeable aluminum battery, ACS Appl. Mater. Interfaces 7 (2015) 24385–24389.
[65] N. Koura, A preliminary investigation for an Al/AlCl3 - NaCl/FeS2 secondary cell, J. Electrochem. Soc. 127 (1980) 1529–1531.
[66] T. Mori, Y. Orikasa, K. Nakanishi, C. Kezheng, M. Hattori, T. Ohta, et al., Discharge/charge reaction mechanisms of FeS2 cathode material for aluminum rechargeable batteries at 55°C, J. Power Sources 313 (2016) 9–14.
[67] S. Wang, Z. Yu, J. Tu, J. Wang, D. Tian, Y. Liu, et al., A novel aluminum-ion battery: Al/AlCl3-[EMIm]Cl/Ni3S2@Graphene, Adv. Energy Mater. 6 (2016) 1600137.
[68] S. Wang, S. Jiao, J. Wang, H.-S. Chen, D. Tian, H. Lei, et al., High-performance aluminum-ion battery with CuS@C microsphere composite cathode, ACS Nano 11 (2017) 469–477.
[69] L. Geng, G. Lv, X. Xing, J. Guo, Reversible electrochemical intercalation of aluminum in Mo6S8, Chem. Mater. 27 (2015) 4926–4929.
[70] K. Liang, L. Ju, S. Koul, A. Kushima, Y. Yang, Self-supported tin sulfide porous films for flexible aluminum-ion batteries, Adv. Energy Mater. 9 (2019) 1802543.
[71] Y. Hu, B. Luo, D. Ye, X. Zhu, M. Lyu, L. Wang, An innovative freeze-dried reduced graphene oxide supported SnS2 cathode active material for aluminum-ion batteries, Adv. Mater. 29 (2017) 1606132.
[72] L. Geng, J.P. Scheifers, C. Fu, J. Zhang, B.P.T. Fokwa, J. Guo, Titanium sulfides as intercalation-type cathode materials for rechargeable aluminum batteries, ACS Appl. Mater. Interfaces 9 (2017) 21251–21257.
[73] Z. Yu, Z. Kang, Z. Hu, J. Lu, Z. Zhou, S. Jiao, Hexagonal NiS nanobelts as advanced cathode materials for rechargeable Al-ion batteries, Chem. Commun. (Camb) 52 (2016) 10427–10430.
[74] X. Zhang, S. Wang, J. Tu, G. Zhang, S. Li, D. Tian, et al., Flower-like vanadium suflide/reduced graphene oxide composite: an energy storage material for aluminum-ion batteries, ChemSusChem 11 (2018) 709–715.
[75] G. Cohn, L. Ma, L.A. Archer, A novel non-aqueous aluminum sulfur battery, J. Power Sources 283 (2015) 416–422.
[76] T. Gao, X. Li, X. Wang, J. Hu, F. Han, X. Fan, et al., A rechargeable Al/S battery with an ionic-liquid electrolyte, Angew. Chem. Int. Ed. 55 (2016) 9898–9901.
[77] H. Yang, L. Yin, J. Liang, Z. Sun, Y. Wang, H. Li, et al., An aluminum–sulfur battery with a fast kinetic response, Angew. Chem. Int. Ed. 57 (2018) 1898–1902.
[78] X. Yu, A. Manthiram, Electrochemical energy storage with a reversible nonaqueous room-temperature aluminum–sulfur chemistry, Adv. Energy Mater. 7 (2017) 1700561.
[79] X. Yu, M.J. Boyer, G.S. Hwang, A. Manthiram, Room-temperature aluminum-sulfur batteries with a lithium-ion-mediated ionic liquid electrolyte, Chem 4 (2018) 586–598.
[80] A. Abouimrane, D. Dambournet, K.W. Chapman, P.J. Chupas, W. Weng, K. Amine, A new class of lithium and sodium rechargeable batteries based on selenium and selenium–sulfur as a positive electrode, J. Am. Chem. Soc. 134 (2012) 4505–4508.
[81] X. Huang, Y. Liu, C. Liu, J. Zhang, O. Noonan, C. Yu, Rechargeable aluminum–selenium batteries with high capacity, Chem. Sci. 9 (2018) 5178–5182.
[82] S. Liu, X. Zhang, S. He, Y. Tang, J. Wang, B. Wang, et al., An advanced high energy-efficiency rechargeable aluminum-selenium battery, Nano Energy (2019) 104159.
[83] J. Jiang, H. Li, T. Fu, B.-J. Hwang, X. Li, J. Zhao, One-dimensional Cu2–xSe nanorods as the cathode material for high-performance aluminum-ion battery, ACS Appl. Mater. Interfaces 10 (2018) 17942–17949.
[84] W. Xing, D. Du, T. Cai, X. Li, J. Zhou, Y. Chai, et al., Carbon-encapsulated CoSe nanoparticles derived from metal-organic frameworks as advanced cathode material for Al-ion battery, J. Power Sources 401 (2018) 6–12.
[85] T. Cai, L. Zhao, H. Hu, T. Li, X. Li, S. Guo, et al., Stable CoSe2/carbon nanodice@ reduced graphene oxide composites for high-performance rechargeable aluminum-ion batteries, Energy Environ. Sci. 11 (2018) 2341–2347.
[86] Y. Du, S. Zhao, C. Xu, W. Zhang, S. Fan, P. Li, et al., Porous α-MnSe microsphere cathode material for high-performance aluminum batteries, ChemElectroChem 6 (2019) 4437–4443.
[87] L.D. Reed, S.N. Ortiz, M. Xiong, E.J. Menke, A rechargeable aluminum-ion battery utilizing a copper hexacyanoferrate cathode in an organic electrolyte, Chem. Commun. (Camb) 51 (2015) 14397–14400.
[88] S. Liu, G.L. Pan, G.R. Li, X.P. Gao, Copper hexacyanoferrate nanoparticles as cathode material for aqueous Al-ion batteries, J. Mater. Chem. 3 (2015) 959–962.
[89] S. Guo, Y. Zhang, Y. Ge, S. Zhang, H. Zeng, H. Zhang, 2D V-V binary materials: status and challenges, Adv. Mater. 31 (2019) 1902352.

[90] G. Li, J. Tu, M. Wang, S. Jiao, Cu3P as a novel cathode material for rechargeable aluminum-ion batteries, J. Mater. Chem. 7 (2019) 8368–8375.
[91] J. Tu, M. Wang, X. Xiao, H. Lei, S. Jiao, Nickel phosphide nanosheets supported on reduced graphene oxide for enhanced aluminum-ion batteries, ACS Sustain. Chem. Eng. 7 (2019) 6004–6012.
[92] B. Xue, Z. Fu, H. Li, X. Liu, S. Cheng, J. Yao, et al., Cheap and environmentally benign electrochemical energy storage and conversion devices based on AlI3 electrolytes, J. Am. Chem. Soc. 128 (2006) 8720–8721.
[93] L. Yu, F.-C. Liu, Z.-W. Fu, Electrochemical features of Al/I2 batteries in water and non-aqueous solution, Electrochim. Acta 54 (2009) 2818–2822.
[94] S. Zhang, X. Tan, Z. Meng, H. Tian, F. Xu, W.-Q. Han, Naturally abundant high-performance rechargeable aluminum/iodine batteries based on conversion reaction chemistry, J. Mater. Chem. 6 (2018) 9984–9996.
[95] T. Nestler, E. Roedern, F. Uvarov Nikolai, J. Hanzig, G. Antonio Elia, M. de Vivanco, Separators and electrolytes for rechargeable batteries: fundamentals and perspectives, Phys. Sci. Rev. 4 (2018) 20170115.
[96] H. Chen, H. Xu, B. Zheng, S. Wang, T. Huang, F. Guo, et al., Oxide film efficiently suppresses dendrite growth in aluminum-ion battery, ACS Appl. Mater. Interfaces 9 (2017) 22628–22634.
[97] H. Wang, S. Gu, Y. Bai, S. Chen, F. Wu, C. Wu, High-voltage and noncorrosive ionic liquid electrolyte used in rechargeable aluminum battery, ACS Appl. Mater. Interfaces 8 (2016) 27444–27448.
[98] H. Wang, S. Gu, Y. Bai, S. Chen, N. Zhu, C. Wu, et al., Anion-effects on electrochemical properties of ionic liquid electrolytes for rechargeable aluminum batteries, J. Mater. Chem. 3 (2015) 22677–22686.
[99] S. Sang, Y. Liu, W. Zhong, K. Liu, H. Liu, Q. Wu, The electrochemical behavior of TiO2-NTAs electrode in H+ and Al3+ coexistent aqueous solution, Electrochim. Acta 187 (2016) 92–97.
[100] M. Kazazi, P. Abdollahi, M. Mirzaei-Moghadam, High surface area TiO2 nanospheres as a high-rate anode material for aqueous aluminium-ion batteries, Solid State Ion. 300 (2017) 32–37.
[101] A. Zhou, L. Jiang, J. Yue, Y. Tong, Q. Zhang, Z. Lin, et al., Water-in-Salt electrolyte promotes high capacity FeFe(CN)6 cathode for aqueous Al-ion battery, ACS Appl. Mater. Interfaces 11 (2019) 41356.
[102] W. Pan, Y. Wang, Y. Zhang, H.Y.H. Kwok, M. Wu, X. Zhao, et al., A low-cost and dendrite-free rechargeable aluminium-ion battery with superior performance, J. Mater. Chem. 7 (2019) 17420–17425.
[103] S. He, J. Wang, X. Zhang, J. Chen, Z. Wang, T. Yang, et al., A high-energy aqueous aluminum-manganese battery, Adv. Funct. Mater. 0 (2019) 1905228.
[104] S.D. Han, N.N. Rajput, X. Qu, B. Pan, M. He, M.S. Ferrandon, et al., Origin of electrochemical, structural, and transport properties in nonaqueous zinc electrolytes, ACS Appl. Mater. Interfaces 8 (2016) 3021–3031.
[105] M. Xu, D.G. Ivey, Z. Xie, W. Qu, Electrochemical behavior of Zn/Zn(II) couples in aprotic ionic liquids based on pyrrolidinium and imidazolium cations and bis(trifluoromethanesulfonyl)imide and dicyanamide anions, Electrochim. Acta 89 (2013) 756–762.
[106] M. Xu, D.G. Ivey, Z. Xie, W. Qu, E. Dy, The state of water in 1-butly-1-methyl-pyrrolidinium bis(trifluoromethanesulfonyl)imide and its effect on Zn/Zn(II) redox behavior, Electrochim. Acta 97 (2013) 289–295.
[107] F. Wang, O. Borodin, T. Gao, X. Fan, W. Sun, F. Han, et al., Highly reversible zinc metal anode for aqueous batteries, Nat. Mater. 17 (2018) 543–549.
[108] C. Zhang, Y. Ding, L. Zhang, X. Wang, Y. Zhao, X. Zhang, et al., A sustainable redox-flow battery with an aluminum-based, deep-eutectic-solvent anolyte, Angew. Chem. Int. Ed. 56 (2017) 7454–7459.
[109] L. Zhang, C. Zhang, Y. Ding, K. Ramirez-Meyers, G. Yu, A low-cost and high-energy hybrid iron-aluminum liquid battery achieved by deep eutectic solvents, Joule 1 (2017) 623–633.
[110] A.P. Abbott, R.C. Harris, Y.-T. Hsieh, K.S. Ryder, I.W. Sun, Aluminium electrodeposition under ambient conditions, Phys. Chem. Chem. Phys. 16 (2014) 14675–14681.
[111] S. Song, M. Kotobuki, F. Zheng, Q. Li, C. Xu, Y. Wang, et al., Al conductive hybrid solid polymer electrolyte, Solid State Ion. 300 (2017) 165–168.
[112] Y. Yamada, J. Wang, S. Ko, E. Watanabe, A. Yamada, Advances and issues in developing salt-concentrated battery electrolytes, Nat. Energy 4 (2019) 269–280.
[113] P. Jiang, L. Chen, H. Shao, S. Huang, Q. Wang, Y. Su, et al., Methylsulfonylmethane-based deep eutectic solvent as a new type of green electrolyte for a high-energy-density aqueous lithium-ion battery, ACS Energy Lett. 4 (2019) 1419–1426.
[114] D. Reber, R.-S. Kühnel, C. Battaglia, Suppressing crystallization of water-in-salt electrolytes by asymmetric anions enables low-temperature operation of high-voltage aqueous batteries, ACS Mater. Lett. 1 (2019) 44–51.
[115] K.N. Wood, E. Kazyak, A.F. Chadwick, K.-H. Chen, J.-G. Zhang, K. Thornton, et al., Dendrites and pits: untangling the complex behavior of lithium metal anodes through operando video microscopy, ACS Cent. Sci. 2 (2016) 790–801.
[116] L. Fan, H. Lu, J. Leng, Z. Sun, C. Chen, The effect of crystal orientation on the aluminum anodes of the aluminum–air batteries in alkaline electrolytes, J. Power Sources 299 (2015) 66–69.
[117] Q. Wang, B. Chen, Q. Zhang, X. Lu, S. Zhang, Aluminum deposition from lewis acidic 1-butyl-3-methylimidazolium chloroaluminate ionic liquid ([Bmim]Cl/AlCl3) modified with methyl nicotinate, ChemElectroChem 2 (2015) 1794–1798.
[118] A.P. Abbott, F. Qiu, H.M.A. Abood, M.R. Ali, K.S. Ryder, Double layer, diluent and anode effects upon the electrodeposition of aluminium from chloroaluminate based ionic liquids, Phys. Chem. Chem. Phys. 12 (2010) 1862–1872.
[119] L. Suo, D. Oh, Y. Lin, Z. Zhuo, O. Borodin, T. Gao, et al., How solid-electrolyte interphase forms in aqueous electrolytes, J. Am. Chem. Soc. 139 (2017) 18670–18680.
[120] L. Suo, O. Borodin, W. Sun, X. Fan, C. Yang, F. Wang, et al., Advanced high-voltage aqueous lithium-ion battery enabled by "water-in-bisalt" electrolyte, Angew. Chem. Int. Ed. 55 (2016) 7136–7141.
[121] F. Wang, Y. Lin, L. Suo, X. Fan, T. Gao, C. Yang, et al., Stabilizing high voltage LiCoO2 cathode in aqueous electrolyte with interphase-forming additive, Energy Environ. Sci. 9 (2016) 3666–3673.
[122] D. Yuan, W. Manalastas Jr, L. Zhang, J.J. Chan, S. Meng, Y. Chen, et al., Lignin@Nafion membrane enabled Zn SEI formation enhancing cycle-life for rechargeable zinc ion battery, ChemSusChem 0. 12 (2019) 4889.
[123] S. Zhao, B. Han, D. Zhang, Q. Huang, L. Xiao, L. Chen, et al., Unravelling the reaction chemistry and degradation mechanism in aqueous Zn/MnO_2 rechargeable batteries, J. Mater. Chem. 6 (2018) 5733–5739.
[124] F. Wan, L. Zhang, X. Dai, X. Wang, Z. Niu, J. Chen, Aqueous rechargeable zinc/sodium vanadate batteries with enhanced performance from simultaneous insertion of dual carriers, Nat. Commun. 9 (2018) 1656.
[125] Z. Li, S. Ganapathy, Y. Xu, Z. Zhou, M. Sarilar, M. Wagemaker, Mechanistic insight into the electrochemical performance of Zn/VO2 batteries with an aqueous ZnSO4 electrolyte, Adv. Energy Mater. 9 (2019) 1900237.
[126] X. He, B. Yan, X. Zhang, Z. Liu, D. Bresser, J. Wang, et al., Fluorine-free water-in-ionomer electrolytes for sustainable lithium-ion batteries, Nat. Commun. 9 (2018) 5320.
[127] Y. Guo, J. Bae, F. Zhao, G. Yu, Functional hydrogels for next-generation batteries and supercapacitors, Trends Chem. 1 (2019) 335–348.
[128] J. Ye, Y. Cheng, L. Sun, M. Ding, C. Wu, D. Yuan, et al., A green SPEEK/lignin composite membrane with high ion selectivity for vanadium redox flow battery, J. Membr. Sci. 572 (2019) 110–118.
[129] M.D. Tikekar, S. Choudhury, Z. Tu, L.A. Archer, Design principles for electrolytes and interfaces for stable lithium-metal batteries, Nat. Energy 1 (2016) 16114.
[130] J. Ye, L. Xia, C. Wu, M. Ding, C. Jia, Q. Wang, Redox targeting-based flow batteries, J. Phys. D Appl. Phys. 52 (2019) 443001.
[131] J. Zhi, A.Z. Yazdi, G. Valappil, J. Haime, P. Chen, Artificial solid electrolyte interphase for aqueous lithium energy storage systems, Sci. Adv. 3 (2017), e1701010.
[132] S.-B. Son, T. Gao, S.P. Harvey, K.X. Steirer, A. Stokes, A. Norman, et al., An artificial interphase enables reversible magnesium chemistry in carbonate electrolytes, Nat. Chem. 10 (2018) 532–539.
[133] V. Verma, S. Kumar, W. Manalastas Jr, R. Satish, M. Srinivasan, Progress in rechargeable aqueous zinc- and aluminum-ion battery electrodes: challenges and outlook, Adv. Sustain. Syst. 3 (2019) 1800111.
[134] Z. Rong, R. Malik, P. Canepa, G. Sai Gautam, M. Liu, A. Jain, et al., Materials design rules for multivalent ion mobility in intercalation structures, Chem. Mater. 27 (2015) 6016–6021.
[135] C. Pan, R.G. Nuzzo, A.A. Gewirth, ZnAlxCo2–xO4 spinels as cathode materials for non-aqueous Zn batteries with an open circuit voltage of ≤2 V, Chem. Mater. 29 (2017) 9351–9359.
[136] A. Yuan, L. Tian, W. Xu, Y. Wang, Al-doped spinel LiAl0.1Mn1.9O4 with improved high-rate cyclability in aqueous electrolyte, J. Power Sources 195 (2010) 5032–5038.
[137] J. Zhao, H. Ren, Q. Liang, D. Yuan, S. Xi, C. Wu, et al., High-performance flexible quasi-solid-state zinc-ion batteries with layer-expanded vanadium oxide cathode and zinc/stainless steel mesh composite anode, Nano Energy 62 (2019) 94.
[138] H. Ren, J. Zhao, L. Yang, Q. Liang, S. Madhavi, Q. Yan, Inverse opal manganese dioxide constructed by few-layered ultrathin nanosheets as high-performance cathodes for aqueous zinc-ion batteries, Nano Res. 12 (2019) 1347.
[139] X. Gu, J-l Liu, J-h Yang, H-j Xiang, X-g Gong, Y-y Xia, First-principles study of H+ intercalation in layer-structured LiCoO2, J. Phys. Chem. C 115 (2011) 12672–12676.
[140] D. Kundu, B.D. Adams, V. Duffort, S.H. Vajargah, L.F. Nazar, A high-capacity and long-life aqueous rechargeable zinc battery using a metal oxide intercalation cathode, Nat. Energy 1 (2016) 16119.
[141] D. Kundu, S. Hosseini Vajargah, L. Wan, B. Adams, D. Prendergast, L.F. Nazar, Aqueous vs. Nonaqueous Zn-ion batteries: consequences of the desolvation penalty at the interface, Energy Environ. Sci. 11 (2018) 881–892.
[142] R.Y. Wang, B. Shyam, K.H. Stone, J.N. Weker, M. Pasta, H.-W. Lee, et al., Reversible multivalent (monovalent, divalent, trivalent) ion insertion in open framework materials, Adv. Energy Mater. 5 (2015) 1401869.
[143] J. Zheng, Y. Hou, Y. Duan, X. Song, Y. Wei, T. Liu, et al., Janus solid–liquid interface enabling ultrahigh charging and discharging rate for advanced lithium-ion batteries, Nano Lett. 15 (2015) 6102–6109.
[144] H. Pan, Y. Shao, P. Yan, Y. Cheng, K.S. Han, Z. Nie, et al., Reversible aqueous zinc/manganese oxide energy storage from conversion reactions, Nat. Energy 1 (2016) 16039.
[145] W. Sun, F. Wang, S. Hou, C. Yang, X. Fan, Z. Ma, et al., Zn/MnO2 battery chemistry with H(+) and Zn(2+) coinsertion, J. Am. Chem. Soc. 139 (2017) 9775–9778.
[146] S. Kim, K.W. Nam, S. Lee, W. Cho, J.-S. Kim, B.G. Kim, et al., Direct observation of an anomalous spinel-to-layered phase transition mediated by crystal water intercalation, Angew Chem. Int. Ed. Engl. 127 (2015) 15309–15314.
[147] J.-Y. Luo, W.-J. Cui, P. He, Y.-Y. Xia, Raising the cycling stability of aqueous lithium-ion batteries by eliminating oxygen in the electrolyte, Nat. Chem. 2 (2010) 760–765.
[148] R. Benedek, M.M. Thackeray, A. van de Walle, Free energy for protonation reaction in lithium-ion battery cathode materials, Chem. Mater. 20 (2008) 5485–5490.
[149] J. Choi, E. Alvarez, T.A. Arunkumar, A. Manthiram, Proton insertion into oxide cathodes during chemical delithiation, Electrochem. Solid State Lett. 9 (2006) A241–A244.

[150] H. Lahan, S.K. Das, Al3+ ion intercalation in MoO3 for aqueous aluminum-ion battery, J. Power Sources 413 (2019) 134–138.
[151] T. Nestler, F. Meutzner, A.A. Kabanov, M. Zschornak, T. Leisegang, D.C. Meyer, Combined theoretical approach for identifying battery materials: Al3+ mobility in oxides, Chem. Mater. 31 (2019) 737–747.
[152] S. Kumar, R. Satish, V. Verma, H. Ren, P. Kidkhunthod, W. Manalastas, et al., Investigating FeVO4 as a cathode material for aqueous aluminum-ion battery, J. Power Sources 426 (2019) 151–161.
[153] T. Nestler, S. Fedotov, T. Leisegang, D.C. Meyer, Towards Al3+ mobility in crystalline solids: critical review and analysis, Crit. Rev. Solid State Mater. Sci. 44 (2019) 298–323.